KME

CONSORTIUM MATERIALS TECHNOLOGY for demonstration and development of thermal energy processes

New Martensitic Steels for Steam Power Plants with Higher Efficiency

KME 510

Hans-Olof Andrén and Fang Liu

New Martensitic Steels for Steam Power Plants with Higher Efficiency

Hans-Olof Andrén and Fang Liu

KME-510

Preface

The project has been performed within the framework the fifth stage of the material technology research programme KME.

KME, Consortium Materials technology for demonstration and development of thermal energy processes, was established 1997 on the initiative of the Swedish Energy Agency. In the consortium, the Swedish Energy Agency, seven industrial companies and 18 energy companies participate. The programme stage has been financed with 60.2% by participating industrial companies and with 39.8% by Swedish Energy Agency. The consortium is managed by Elforsk.

The programme shall contribute to increasing knowledge to forward the development of thermal energy processes for various energy applications through improved expertise, refined methods and new tools. The programme shall through material technology and process technology developments contribute to making electricity production using thermal processes with renewable fuel more effective. This is achieved by

- Forward the industrial development of thermal processes through strengthen collaboration between industry, academy and institutes.
- Build new knowledge and strengthen existing knowledge base at academy and institutes.
- Coordinate ongoing activities within academy, institutes and industry.

KME's activities are characterised by long term industry relevant research and constitutes an important part of the effort to promote the development of new energy technology with the aim to create an economic, environmentally friendly and sustainable energy system.

Abstract

We have proved that the new concept – to use finely distributed Z-phase to strengthen 12% chromium steels to achieve good corrosion resistance and creep strength for high temperature applications – is feasible. Compared to Nb, Ta is a better candidate to form fine Z-phase precipitates. Cu addition can modify the distribution of Laves phase, and yield desirable impact toughness.

Sammanfattning

Den termiska verkningsgraden hos ångkraftverk begränsas av tillåten ångtemperatur och tryck, som i sin tur bestäms av korrosionsbeständigheten och kryphållfastheten hos tillgängliga stål. Alla försök hittills att överskrida 600-620°C med 11-12% kromstål har misslyckats, och vi förstår nu att anledningen är utskiljningen av en komplexnitrid, Z-fas, efter några års drift. Denna fas är grov och tillväxer på bekostnad av fina VN-utskiljningar, vilket leder till en dramatisk försämring av kryphållfastheten. Detta projekt syftar till att utveckla en ny generation martensitiska kromstål som använder Z-fas som härdande i stället för försvagande fas. De nya stålen har potentialen att användas i ångledningar och överhettare i framtida biobränsleeldade kraftverk med förhöjd driftstemperatur.

Det nära samarbetet mellan Chalmers tekniska högskola, Siemens Industrial Turbomachinery AB och DONG/Danmarks tekniska universitet har lett till att grundläggande kunskap vunnits om de nya Z-fasförstärkta stålen. Ett effektivt informationsutbyte inom den så väsentliga återkopplingen mellan legeringsdesign, mikrostrukturanalys och mekanisk provning har resulterat i en djup förståelse av systemet.

Vi har visat att idén att använda en fin och tät fördelning av Z-fas för att förstärka 12% kromstål är praktiskt genomförbar. Idéprövningslegeringarna (proof-of-concept-legeringarna) uppvisade utmärkt kryphållfasthet, jämförbar med dagens bästa legeringar, trots det mycket högre krominnehållet.

Finjustering av legeringssammansättningen har gjorts för att åtgärda två saker, nämligen att förbättra idéprövningslegeringarnas låga slagseghet vid rumstemperatur, och att införa en "normal" kolhalt för att göra en framtida introduktion av legeringen mer ekonomiskt genomförbar. En väsentlig förbättring av segheten uppnåddes. En något försämrad kryphållfasthet erhölls emellertid i de senast designade legeringarna.

Målet som uppsattes för projektet har framgångsrikt uppfyllts.

Nyckelord: 12% kromstål, Z-fasförstärkning, krypmotstånd, mikrostruktur

Summary

The thermal efficiency of steam power plants is limited by the maximum allowed steam temperature and pressure, which in turn are determined by the corrosion and creep resistance of available steels. All attempts so far to exceed 600-620°C with 11-12% chromium steels have failed, and we now know that the reason is the precipitation of a complex nitride, Z-phase, after a few years of service. This phase is coarse and grows at the expense of fine VN precipitates, leading to a dramatic fall in creep strength. This project aims at developing a new generation of martensitic chromium steels that use Z-phase as a strengthening rather than weakening phase. The new steels have the potential to be used as piping or superheater tubing in future biomass power plants with increased operation temperature.

The close collaboration between Chalmers University of Technology, Siemens Industrial Turbomachinery AB, and DTU/DONG Energy has led to fundamental knowledge gained on the new Z-phase strengthened steels. The efficient exchange of information within the essential feedback loop between alloy designing, microstructure analyses, and mechanical testing have resulted in a deep understanding of the system.

We have proved that the concept of using fine and densely distributed Z-phase to strengthen 12% chromium steel is feasible. Despite their much higher chromium content the proof-of-concept alloys showed excellent creep resistance, comparable with benchmark alloys.

Further fine tune of the alloy chemical composition were performed to address two issues: firstly to improve the room temperature impact toughness of the proof-of-concept alloy; secondly to introduce a "normal" amount of carbon into the alloy and make the future implementation of the alloy more economically viable. Significant improvement in toughness has been achieved. However, slightly compromised creep strength was found in the newly designed alloys.

The goal set for the project has been successfully fulfilled.

Keywords: 12%Cr steels, Z-phase strengthening, creep resistance, microstructure

Table of contents

1 Introduction

Design of a new generation of steels with significantly improved corrosion and creep resistance at 650°C/325 bar promises increasing thermal efficiency in thermal power plants, and thus both an improved efficiency in biomass fired plants and a potential annual saving in CO_2 emissions from fossil-fired plants on an order of several gigatonnes globally. With the joint efforts of this project as well as other three closely related projects, we are aiming at designing and gaining understanding of a novel 12% chromium steel system – Z-phase strengthened steels.

1.1 Background

Fossil fired power plants provide more than 70% of the World's electricity and account for about one third of global CO_2 emissions, which reached an all-time high of 34 gigatonnes (Gt) in 2011 [1, 2]. A transition from fossil power plants to renewable energy sources is desirable from an environmental point of view. Combustion of biomass has shown great potential to combat CO_2 emission. This process is often labelled as "zero emission", since the biomass has to bind up CO_2 during the growth.

Compared to the state of the art fossil-fired power plants, biomass fired power plants are run at a much lower temperature, due to severe corrosion attack to the fireside of the superheaters. For these power plants, focus is put on enhancing plant efficiency, mainly through increasing operating steam temperature and pressure. At the same time, we have to keep the construction and maintenance cost as low as possible, in order to make energy produced in these plants attractive to the energy consumers.

High temperature properties of the materials for the crucial components like superheaters in boilers set the limit on the possible improvement of efficiency in these plants. The materials must be capable of being operated at high temperatures and stresses for prolonged time. Hence, degradation mainly due to creep and corrosion must be minimized. For biomass fired power plants, the nearest goal is to increase the steam temperature to 600°C, which means that the temperature of the metal in the superheater is around 630-650°C. Tempered martensitic 9–12% chromium steels offer an optimal combination of the critical properties, i.e. creep strength, corrosion resistance at the steam-side, at a relatively low cost. Therefore, with a proper coating at the fireside, a new generation of 9–12% chromium steels, which possesses high creep strength and steam corrosion resistance at 650°C, can provide reliable and relatively cheap superheaters for the biomass fired power plants.

In this project we performed systematic research in order to gain a comprehensive understanding on the mechanical properties in particular creep properties of these steels, and we provided fundamentally important knowledge, which has been fed into the improvement of the new steels.

1.2 Description of the research field

1.2.1 Microstructure of conventional 9-12%Cr steels and creep resistance

Tempered martensitic steels are usually subject to austenitizing followed by tempering heat treatment. They exhibit a typical microstructure, which consists of prior austenite grain boundaries, blocks, laths, high density of dislocations and precipitates. In the technically interesting stress and temperature range for these steels, the main creep mechanism is dislocation creep. Therefore, the ways to retard or delay dislocation glide and climb are helpful to improve creep resistance [3]. The most important strengthening mechanism is precipitation hardening [4].

The size and number density of the precipitates at the initial stage, as well as their stability against coarsening during exposure to high temperatures play a vital role in creep. The most important precipitates are carbide $M_{23}C_6$ (M = Fe, Cr, Mo), nitride MN (M = V, Nb, Cr) [4], intermetallic Laves phase Fe_2M (M = Mo, W), and complex nitride Z-phase (Cr,Fe)MN (M = V, Nb, Ta).

$M_{23}C_6$ precipitates are the major strengthening particles for the first generation of 9-12%Cr steels like X20CrMoV121. They are mainly located at the prior austenite grain boundaries and lath boundaries, with a typical size of 100 nm after tempering and a few hundred nanometres after prolonged exposure. At late 1970's, researchers at Oak Ridge National Laboratory succeeded in obtaining very fine distributed MN precipitates by adding very small amount of V or Nb and N into the famous alloy – ASTM grade P91. And a few years later, another commercial steel ASTM grade P92, which has similar chemical composition as P91 but adding W and B, was launched. P91 and P92 are mainly based on particle strengthening with MN and $M_{23}C_6$. Compared to $M_{23}C_6$, MN has a much smaller particle size, usually at the range of 20 nm after tempering, and higher number density and more significantly they are very stable against coarsening in P91 and P92 [5]. This makes P92 two times as strong as the old X20CrMoV121 at 600°C.

Laves phase may form in Mo or W containing steels. It has a long nucleation and growth phase at 600°C. W containing Laves phase nucleates faster, thus leading to finer and more densely distributed precipitates.

1.2.2 Z-phase formation and strength breakdown

P92 contains only 9 wt.% Cr, which is too low in terms of corrosion resistance at 650°C. It has been established that at high temperatures the corrosion resistance of a steel is proportional to its Cr content; the higher the Cr content, the better the corrosion resistance [6]. Therefore there have been several recent trials aiming for improving both creep and corrosion properties by adding e.g. Co, W and B to the steels, in combination with a higher Cr content (11-12% vs. 9% in P92). Nevertheless, all of them turned out to be failures. Although they showed better creep resistance at 650°C than older steels until ~10,000 hours, they then suffered a dramatic loss of creep strength [7].

There was debate on the mechanisms behind the dramatic breakdown. Now it is widely accepted that this is mainly attributed to the precipitation of a complex nitride known as Z-phase ((Cr,Fe)(Nb,V) N) during creep. Many small MN precipitates are dissolved to form large Z-phase particles, which are thermodynamically more stable at this temperature but give very little contribution to creep strength [8, 9]. Z-phase formation in a number of 9-12%Cr steels, which rely mainly on MN for strengthening, has been systematically studied. It has been shown that a Cr content above 10.5% strongly accelerates Z-phase formation. In contrast steels with 9% Cr or below are largely unaffected by the Z-phase precipitation up to 100,000 hours at 600-650°C [10].

1.2.3 New 12%Cr martensitic steels with Z-phase as strengthening precipitates

Z-phase precipitates were credited as beneficial for strengthening in creep resistant austenitic steels containing Nb, since they precipitate quickly among the first appearing precipitates and as fine densely distributed particles [11].

Within the European COST 536 ACCEPT (alloys development for critical components of environmentally friendly steam power plant) action, Hald and Danielsen from the Technical University of Demark (one of the collaboration partners in the present project) proposed a new alloy design concept, which makes use of Z-phase as strengthening dispersion for 9-12%Cr martensitic steels, instead of MN. The new steels are supposed to be strengthened by fine Z-phase precipitates, which are formed during heat treatment or at the early stage of application. Good creep resistance would be expected, if densely distributed fine Z-phase precipitates can be formed during heat treatment and if they coarsen slowly during service.

1.3 Research task

Our task was to assist the European development of new 12% chromium steels for use up to 650°C by studying the microstructure and mechanical behaviour of Z-phase strengthened alloys. The alloys were to be provided by DTU (sponsored by DONG energy). The work was to be performed by high-resolution microscopy and microanalysis (SEM, TEM, and APT) at Chalmers, Göteborg, and mechanical and creep testing at Siemens, Finspång.

Within the frame of this project we planned to:

- Select test steels;
- Creep test promising test steels;
- Understand mechanisms of accelerated Z-phase formation by Ta addition;
- Understand effects of small addition of B on the Z-phase strengthened steels;
- Understand microstructure of Z-phase strengthened steels with different heat treatments.

1.4 Goal

The long term goal of this project was to provide fundamentally important knowledge on the sophisticated process-microstructure-properties relationships, which can be fed into the improvement of the new steels so that this new steels with optimal combination of corrosion and mechanical properties can be exploited for use in thermal power plants.

1.5 Project organisation

1.5.1 Industry reference and financing

Siemens Industrial Turbomachinery AB (Lennart Johansson) participated in the project, and performed in-kind work (tensile testing, impact toughness testing, creep testing, reporting and travel) at a planned cost of 1,200,000 SEK during 2010-2013 (reported costs have been 1,540,969 SEK).

DONG Energy (John Hald) participated in the project, and performed in-kind work (providing test melts, working actively with alloy designing, and EBSD analysis of the alloys) at a planned cost of 800,000 SEK during 2010-2013.

This amount covered seven testing melts, and Hald's working hours, in total during 2010-2013.

Additional financing was received from the Research Foundation of VGB (2011-2013, 75 kEUR) and Energimyndigheten (2011-2013, 2,565 kSEK), and the EU-FP7 (2013-2015, 388 kEUR).

1.5.2 Staff

Professor Hans-Olof Andrén at Chalmers University of Technology, works 10% in this project, Assistant Professor Fang Liu (woman), and Ph.D student Masoud Rashidi (from May 2013) at Chalmers University of Technology, works 100% in this project.

Lennart Johansson from Siemens Industrial Turbomachinery AB, John Hald from DONG Energy (until Dec. 2012) / DTU (from 2013), and Hilmar Danielsen (until 2012) also participated in the project.

1.5.3 Project meetings

Regular project meetings have been held through the project period. Every 4 months all participants attend the meeting. Chalmers, DTU and Siemens host the meetings in turn. A brief of all project meetings are listed below.

- **The first project meeting** was hold at Chalmers, Gothenburg, on 12th January 2011.

All project participants, i.e. Fang Liu, Hans-Olof Andrén, John Hald, Hilmar Danielsen and Lennart Johansson attended the meeting. Professor Göran Wahnström and Dan Fors, from the Department of Applied Physics at Chalmers also attended the meeting. Results from all parties were presented. A working plan was agreed by all parties.

- **The second project meeting** was hold at Chalmers, Gothenburg, on 2nd May 2011.

All project participants, i.e. Fang Liu, Hans-Olof Andrén, John Hald, Hilmar Danielsen and Lennart Johansson attended the meeting. Professor Göran Wahnström, from the Department of Applied Physics at Chalmers also attended the meeting. Results from all parties were presented. A working plan was agreed upon by all parties.

- **The third project meeting** was hold at Siemens, Finspång, on 10th October, 2011.

All project participants, i.e. Fang Liu, Hans-Olof Andrén, John Hald, Hilmar Danielsen and Lennart Johansson attended the meeting. Results from all parties were presented. A working plan was agreed upon by all parties.

- **The fourth project meeting** was at DONG Energy, Copenhagen on 24th January 2012.

All project participants, i.e. Fang Liu, Hans-Olof Andrén, John Hald, Trine Lomholt, Hilmar Danielsen and Lennart Johansson attended the meeting. Results from all parties were presented. A working plan was agreed upon by all parties.

- **The fifth project meeting** was hold at Chalmers University of Technology, Gothenburg, on the 12th June, 2012.

All project participants, i.e. Hans-Olof Andrén and Fang Liu from Chalmers, John Hald, Trine Lomholt and Hilmar Danielsen from DTU, and Lennart Johansson from Siemens, attended the meeting. Results from all parties were presented. A working plan was agreed upon by all parties.

- **The sixth project meeting** was hold at Siemens Industrial Turbomachinery, Finspång, on the 19th October, 2012.

Project participants, i.e. Hans-Olof Andrén and Fang Liu from Chalmers, John Hald from DTU, and Lennart Johansson from Siemens attended the meeting. Results from all parties were presented. A working plan was agreed upon by all parties.

- **The seventh project meeting** was hold at the Technical University of Denmark, on 4th April, 2013.

Project participants, i.e. Hans-Olof Andrén, Fang Liu and Masoud Rashidi from Chalmers, John Hald from DTU, and Lennart Johansson from Siemens attended the meeting. Results from all parties were presented. A working plan was agreed upon by all parties.

- **The eighth project meeting** was hold at Chalmers University of Technology, on 22nd August, 2013.

Project participants, i.e. Hans-Olof Andrén, Fang Liu and Masoud Rashidi from Chalmers, John Hald from DTU, and Lennart Johansson from Siemens attended the meeting. Results from all parties were presented. A working plan was agreed upon by all parties.

- **The ninth project meeting** was hold at Siemens Industrial Turbomachinery, Finspång, on the 4th December 2013.

Project participants, i.e. Hans-Olof Andrén, Fang Liu and Masoud Rashidi from Chalmers, John Hald from DTU, and Lennart Johansson from Siemens attended the meeting. Results from all parties were presented. A working plan was agreed upon by all parties.

1.5.4 Communication

A web-based communication tool has been set up, minutes and presentations from all the project meetings are available for all participants on an internal website.
Results from the project have been presented at the 8th International Charles Parsons Turbine Conference, Portsmouth, UK, 5-8 September 2011, at the 2nd International Conference on Super-High Strength Steels, Peschiera del Garda, Italy, 17-20 October 2011, and at the EPRI 7th International Conference on Advances in Materials Technology for Fossil Power Plants, Hawaii, USA, 22-25 October, 2013, and will be presented at the 10th Liège Conference on Materials for Advanced Power Engineering, Liège, Belgium, 14-17 September, 2014.

The results have also been published in high-quality scientific journals, see Chapter 9.

2 Work layout

For the first stage of the project, test materials (Z1, Z2, Z3 and Z4 steels) were designed and provided by DONG Energy (Section 3.1). Systematic heat treatment variations were performed by Siemens (Section 3.2), and then detailed microstructure analysis was carried out at Chalmers (Section 3.3), aiming at identifying the best heat treatment conditions. With the optimal heat treatment condition determined, the alloys underwent proper heat treatment and were mechanically tested (tensile testing, hardness testing, impact toughness testing, and creep testing) by Siemens (Section 3.2). Chalmers made detailed microstructural investigations on the mechanical tested alloys, in particular those that had undergone long-term high temperature aging and creep (Section 3.3).

Two of the first testing alloys with 12%Cr, i.e. Z3 and Z4, showed very good creep resistance, comparable to the best commercial 9%Cr steels used today. Thus it has been proved that the concept of using Z-phase to strengthen the steels works. However, the first trial steels exhibited poor impact toughness (Section 3.2). The reason behind this was identified by microstructural analysis (Section 3.3.).

With this feedback, for the second stage of the project, DONG designed a new series of alloys (the ZL series), and produced melts of the new alloys (section 3.1.). These alloys have more economically "realistic" chemical composition, in terms of carbon and expensive alloying elements content. Mechanical testing be Siemens showed that they have optimal mechanical properties, in particular much improved impact toughness (Section 3.2.). Microstructure of them has been investigated (Section 3.2.) at Chalmers.

3 Results

3.1 Alloy design

Alloy design was guided by modelling (performed mainly by DONG Energy / DTU) in combination with a continuously deepened understanding of the correlation between mechanical properties (tested mainly by Siemens) and the microstructure (investigated mainly by Chalmers) of this new alloy system. In the first stage of the project, we produced four proof-of-concept alloys; we chose two of them that showed δ-ferrite-free microstructure, high tensile strength, sufficient ductility, and most significantly very promising creep strength. However, their impact toughness was poor. In the second stage of the project, we improved alloy designing by adding Cu (~1at.%) and Mo to modify Laves phase; and increasing the content of the cheap austenite stabilizer carbon. Optimized mechanical properties were achieved.

3.1.1 Proof of concept

To prove the concept of Z-phase strengthening we started with four test alloys with simplified chemical composition. To avoid the formation of carbides and possibly lose Ta or Nb in forming carbides rather than Z-phase, the first alloys had a low carbon content. For alloy designing the aspects that we put special emphasize on are: the balance between Z-phase forming elements: i.e. Ta/Nb and N, to maximize precipitation strengthening; and the balance between austenite forming (C, N, Co, Ni and Mn) and ferrite forming (Fe, Cr, Ta, Nb and Si) elements to avoid the formation of detrimental δ-ferrite. The first two test alloys Z1 and Z2 contained more than 5% δ-ferrite (***Figure 3-1***). The test alloys Z3 and Z4 were almost free of δ-ferrite. Alloy Z3 forms CrNbN, and Z4 forms CrTaN. The chemical compositions of the four alloys are listed in ***Table 3-1***. We found densely dispersed Z-phase precipitates in these two alloys (see Section 3.4). The creep strength of them is excellent. All other mechanical properties are good, except for toughness (see Section 3.3).

Table 3-1. *Nominal composition of the test Z-strengthened steels Z1, Z2, Z3 and Z4 (in* ***atomic*** *percent, and Fe in balance).*

Steel	Ni	Co	Cr	W	Nb	Ta	Cu	Mo	C	B	N	Si	Mn
Z1	0.59	2.86	12.94	0.73	0.24	-	0.93	0.09	0.02	0.04	0.24	0.72	0.52
Z2	0.45	4.69	12.80	0.75	0.17	-	0.83	0.13	0.01	0.02	0.16	0.62	0.48
Z3	1.41	5.17	12.64	0.87	0.16	-	-	-	0.02	0.02	0.15	0.6	0.50
Z4	0.48	7.01	12.84	0.89	-	0.12	-	-	0.02	0.02	0.13	0.6	0.49

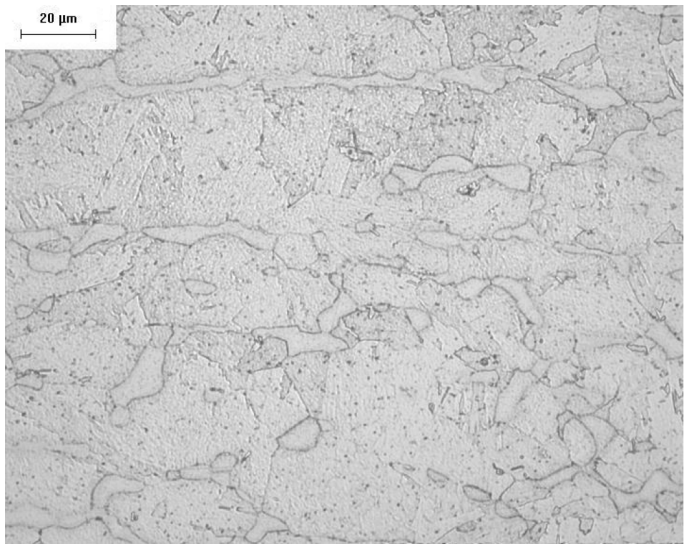

(a)

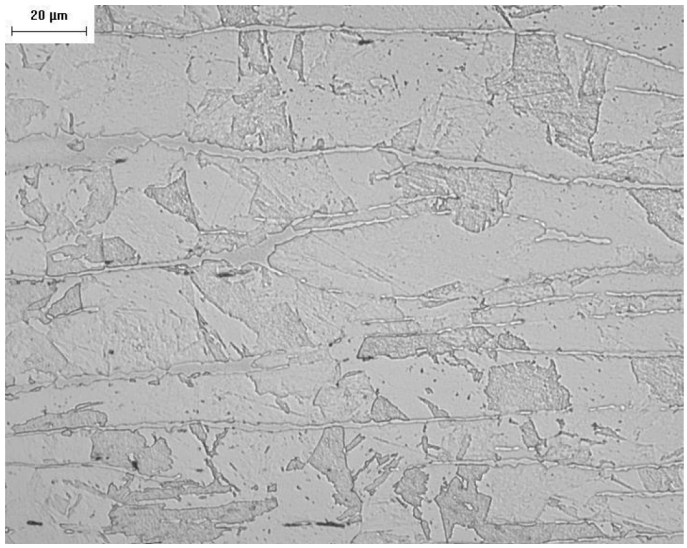

(b)

Figure 3-1. Optical micrographs showing δ-ferrite in (a) Z1 as nodules; and (b) Z2 as continuous strips.

3.1.2 Further alloy design optimization

Further alloy design optimization is mainly based on two concerns: firstly to improve impact toughness of the steel; and secondly to reduce utilization of the costly austenite stabilizer, Co, by increasing the C content. The chemical compositions of the new series of alloys are listed in ***Table 3-2***.

3.1.2.1 Cu and Mo addition

The poor room temperature impact toughness of the simplified alloy systems (Z3 and Z4) was found to be due to the formation of continuous Laves phase along prior austenite grain boundaries (Section 3.4.6.1). Therefore we modified the alloy design by adding Cu and/or Mo. This is the base for the ZL series steels, which have, otherwise, similar chemical composition as the Z4 steel. This alloy composition modification is based on our previous experience that Cu can greatly influence the formation of Laves phase [12]. Due to Cu addition, special heat treatment procedure was designed (Section 3.2.2). Much improved Charpy V-notch testing results were obtained for the modified alloys (Section 3.3.1).

3.1.2.2 Carbon addition

At the first stage of the project, in order to test the concept of Z-phase strengthening, we kept the carbon concentration very low so that the possible formation of various carbides, such as Ta(C,N)/Nb(C,N) or $M_{23}C_6$, was avoided to a large extent. Thus, we could definitely isolate and identify the strengthening effect of Z-phase. However, to keep the carbon concentration as low as ~ 50 ppm, extra processes must be performed during steel manufacturing. In addition, carbon is a very cheap austenite stabilizer compared with Co and Cu. Therefore, in order to make the new alloys more economically viable, "normal" amount of carbon was added into one of the new ZL steels, ZL3. As expected formation of both Z-phase, Ta(C,N) and $M_{23}C_6$ was observed (Section 3.4.6.2).

Table 3-2. *Nominal composition of the test Z-phase strengthened steels ZL1, ZL2 and ZL3 (in* ***atomic*** *percent, and Fe in balance).*

Steel	Ni	Co	Cr	W	Ta	C	B	N	Si	Mn	Cu	Mo
ZL1	0.99	6.22	13.00	0.76	0.12	0.02	0.04	0.23	0.58	0.58	0.89	0.12
ZL2	1.02	6.26	13.03	0.76	0.12	0.02	0.01	0.22	0.62	0.48	0.02	0.12
ZL3	0.18	3.35	13.13	0.76	0.11	0.28	0.03	0.20	0.62	0.22	1.73	-

3.2 Heat treatment optimization

For 9-12%Cr steels heat treatment plays an important role in dictating their creep properties. The typical heat treatment procedures are:

- Austenitization (sometimes also called normalization) at > 1000°C;
- Quenching, usually in air, to obtain a martensitic structure with supersaturated carbon. At this stage the steel has very high strength, but is too brittle to be used.
- Tempering at 700-800°C. At this stage precipitation of nano-sized strengthening particles takes place. The hardness of the steel decreases dramatically.

The aim is, by performing systematic investigation, to provide a guideline of heat treatment for the new martensitic steels. This practical guideline ensures an optimal combination of strength, ductility, and toughness.

3.2.1 Heat treatment for test alloys Z3 and Z4

3.2.1.1 Heat treatment and hardness testing

In order to find the most suitable heat treatment conditions, a matrix of different combinations of austenitization and tempering temperatures was tested. Three different austenitization temperatures, 1050°C, 1100°C and 1150°C, were used for both Z4 and Z3. Holding time at the austenitization temperature was always 1 hour. For Z4, two tempering temperatures, i.e. 720°C and 740°C, were chosen. For each austenitization and tempering temperature combination, three holding periods were applied; for tempering at 720°C, they were 6, 24 and 96 hours; for 740°C they were 4, 16 and 64 hours. Z3 was only tempered at 720°C with holding time of 6, 24 and 96 hours. Hardness of the steels after each heat treatment was measured.

Hardness values as a function of tempering time are shown in ***Figures 3-2*** **(a), (b)** and **(c)** for austenitization temperature 1050°C, 1100°C, and 1150°C, respectively. All curves show exactly the same trend: very high hardness for the as-quenched condition; during tempering the hardness value drops down remarkably for the first 4 or 6 hours. After that, hardness increases gradually with time until 64 or 96 hours. For the same tempering conditions, the hardness values are higher for higher austenitization temperatures. This is true for both as quenched materials and tempered materials. A minimum hardness value was found after 6-12 hours tempering.

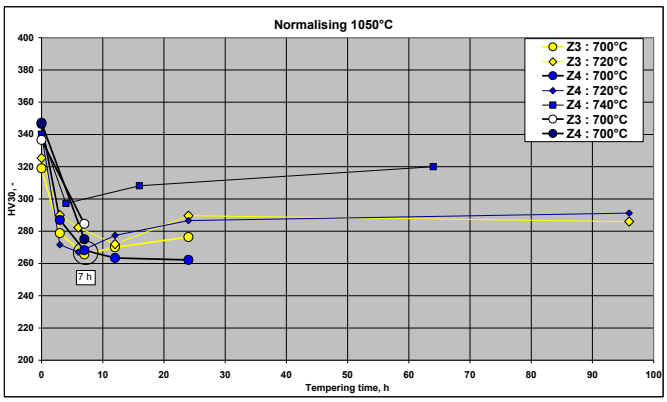

(a)

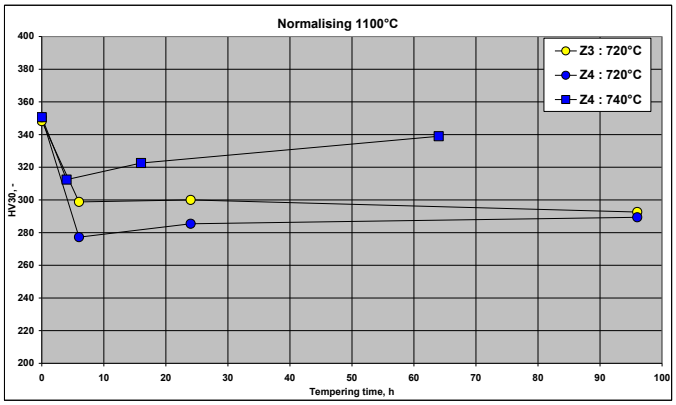

(b)

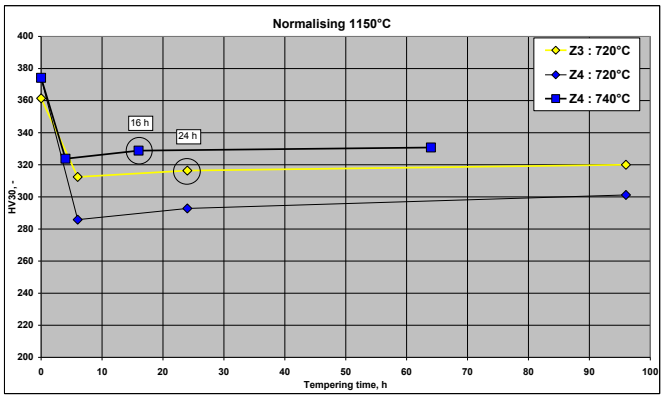

(c)

Figure 3-2. *Hardness of the Z3 and Z4 testing steels after different heat treatment as a function of tempering time. (a) Austenitization at 1050°C. (b) Austenitization at 1100°C. (c) Austenitization at 1150°C. (The lines are only to guide the eye.)*

3.2.1.2 Metallurgical analysis for samples undergone different heat treatment conditions

Metallurgical analysis was performed on fine-polished samples, in order to find out the influence of heat treatment condition on the microstructure of the steels, specifically their average prior austenite grain (PAG) size. We used mean linear intercept method (ASTM Standard E112-12) to determine the average size of PAGs based on SEM backscattered-electron images. When the grain sizes were big (>30 micrometres), a series of 4 × 4 matrix of images were taken and analysed to make sure that enough grains were present in the same field of view.

Figure 3-3 shows SEM images of Z4 and Z3 heat treated at 1050°C 1h + 720°C 6h and 1150°C 1h + 720°C 6h. Since they contain much of the heavy element W, Laves phase (Fe_2W) precipitates give bright contrast in back-scattered images. These precipitates heavily decorate PAG boundaries, thus making the PAGs clearly visible.

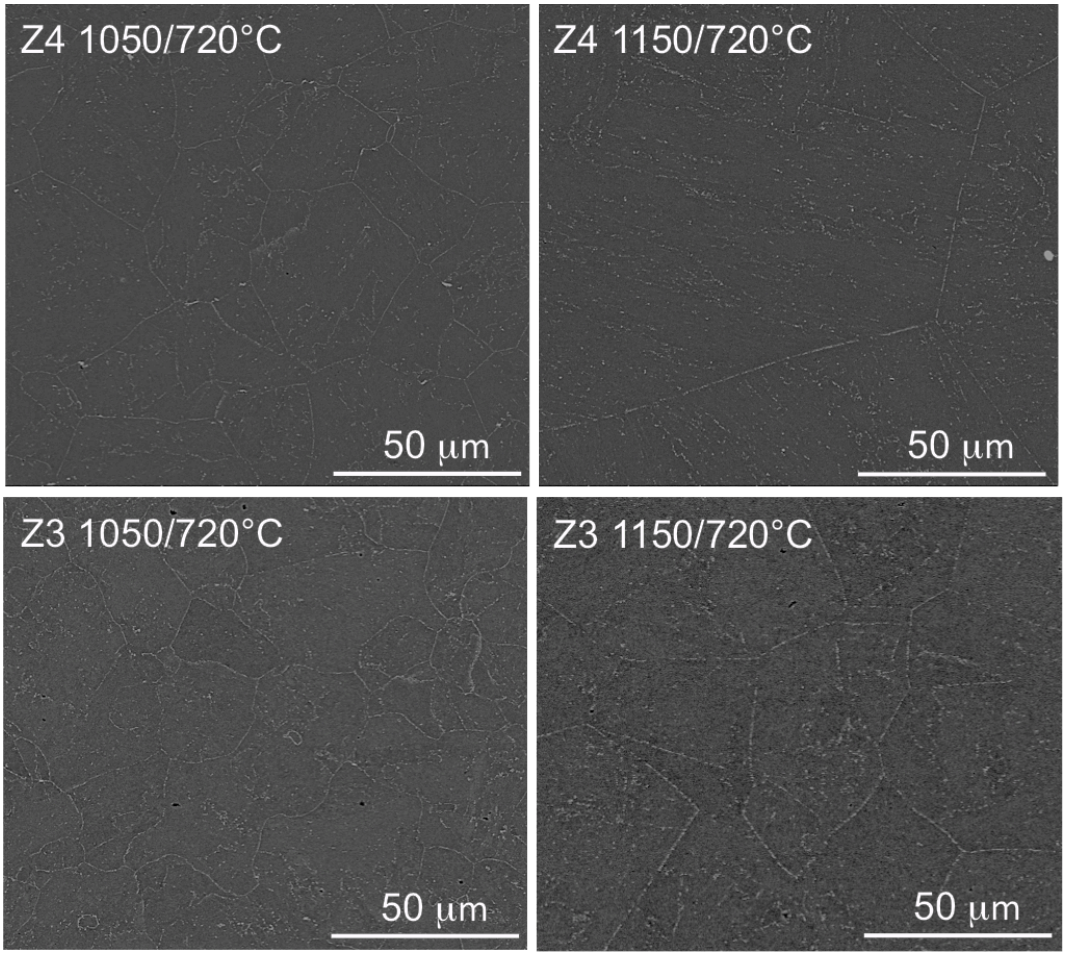

Figure 3-3. *SEM backscattered-electron micrographs of Z4 and Z3 (heat-treated at 1050°C 1h + 720°C 6h and 1150°C 1h + 720°C 6h).*

The average PAG sizes are given in ***Table 3-3***. The errors were given by standard error of 2σ on the average grain size (NOT individual size). The average PAG size increases with increasing austenitization temperature. In the Z4 steel, the average size is around five times bigger when the austenitization temperature is 1150°C compared with 1050°C. However, this effect is much less significant in the Z3 steel; the average size in about two times bigger when the austenitization temperature is 1150°C compared with 1050°C.

Table 3-3. *Average prior austenite grain size in Z3 and Z4 subjected to different heat treatment.*

Samples	Austenitization T	Tempering T/time	Grain size (95% confidence level)
Z4	1050°C	720°C/6h	21.9 ± 3.2
Z4	1150°C	720°C/6h	114 ± 4.2
Z3	1050°C	720°C/6h	24.3 ± 8.9
Z3	1150°C	720°C/6h	57.6 ± 34.9

3.2.2 Heat treatment of the ZL series

Since we have already knowledge gained on heat treatment from Z3 and Z4 steels, together with our previous experience on 9-12%Cr steels, the heat treatment conditions for the new alloy series ZL series was designed to be: austenitization temperature at 1150°C, and then a two-stage tempering: 650°C 6 h + 740/700°C 6 h.

We chose a high austenitization temperature 1150°C instead of 1050°C, in order to dissolve as many primary TaC as possible, and make more Ta available for forming Z-phase in subsequent heat treatment. During the two-stage tempering, the first stage allows part of the Cu to precipitate out of the ferrite matrix, and this will increase the A_1 temperature of the remaining steel matrix. With an increased A_1 temperature, the second stage tempering can be carried out at a higher temperature. Specifically for the steel ZL3, which has a higher C content, and thus a higher A1 temperature, a tempering temperature as high as 740°C is possible without the risk of austenite re-formation. On the other hand, to facilitate precipitation of very fine strengthening particles a low tempering temperature of 700°C was also used.

Different second stage tempering temperature resulted in different yield strength. ZL3 that was heat-treated by 1150°C/1h + 650°C/6h + 740°C/6h exhibits a lower yield strength, and is therefore referred to as ZL3 LY (low yield). ZL3 that was heat-treated by 1150°C/1h + 650°C/6h + 700°C/6h exhibits a higher yield strength, and is therefore referred to as ZL3 HY (high yield) (see also Section 3.3.1).

Table 3-4. *Average prior austenite grain size in ZL3 in comparison with Z4.*

Samples	**Austenitization T**	**Tempering T/time**	**Grain size (95% confidence level)**
Z4	1150°C	720°C/6h	114 ± 4.2
ZL3 LY	1150°C	650°C/6h+ 740°C/6h	24.3 ± 8.9

3.3 Mechanical testing

For future applications, besides good long-term mechanical properties and corrosion resistance at elevated temperatures, all the test alloys must possess reasonable mechanical properties at room temperature.

3.3.1 Room temperature tensile and impact testing

Tensile and impact testing were performed on Z3 and Z4 samples that were austenitized at 1050°C and then tempered at 700°C for 7 hours. The results are shown in ***Table 3-5***. Both steels exhibited very good tensile strength and ductility. However, they showed very poor impact toughness. We believe that the reason behind this lies the microstructure: preferential segregation of W and/or consequently precipitation of Laves phase particles along prior austenite grain boundaries and lath boundaries were responsible for the poor impact strength for Z3 and Z4. The detailed micrograph and microanalysis is presented in Section 3.4.6.1.

As mentioned in the Section 3.1.2 "Further Alloy Design Optimization", to tackle this problem we tested a new series design of test steels with Cu (~2 at.%) and Mo additions that aim at modifying the Laves phase.

Mechanical and impact testing results for ZL series alloys are also displayed in ***Table 3-5***. The impact strength for ZL1, ZL2 and ZL3 are greatly improved upon Z3 and Z4. We believe that this depends on the Cu and Mo additions. ZL2 contains much less Cu, therefore the Laves phase formation is more like that in Z4, and thus poorer impact toughness results.

Table 3-5. *Tensile and impact testing results for the test alloys.*

Material	Aust. T (°C)	Temp. T (°C)	Temp. time (h)	Rp (MPa)	Rm (MPa)	A5 (%)	Z (%)	KV (J)
Z3	1050	700	7	647	798	18.0	70.8	3.3
Z4	1050	700	7	770	890	16.0	67.4	3.0
ZL1	1050	700	7	–	–	–	–	46.3
ZL2	1050	700	7	–	–	–	–	21
ZL3 LY	1150	650+740	6	694	805	19.7	66.3	76.3
ZL3 HY	1150	650+700	6	846	944	16.3	62.1	29

The mechanical testing results for the two heat treatment varieties for ZL3 are also displayed in ***Table 3-5***. ZL3 that was heat treated by 1150°C/1h + 650°C/6h + 740°C/6h exhibits a lower yield strength, and is therefore referred to as ZL3 LY (low yield). ZL3 that was heat treated by 1150°C/1h + 650°C/6h + 700°C/6h exhibits a higher yield strength, and is therefore referred to as ZL3 HY (high yield). ZL3 LY has excellent toughness properties (76 J) and ZL3 HY has acceptable toughness properties (29 J).

3.3.2 Elevated temperature tensile testing

For future applications at high temperatures the steels must also possess reasonable strength at elevated temperatures. Therefore, tensile testing at elevated temperatures was performed on the alloy ZL3 with improved toughness. The results are promising as shown in ***Figure 3-4 (a)*** and ***(b)*** for two heat treatment varieties of ZL3, ZL3 LY and ZL3 HY, respectively, and for comparison the strength of the benchmark alloy ASTM grade P91 is also given in the figures.

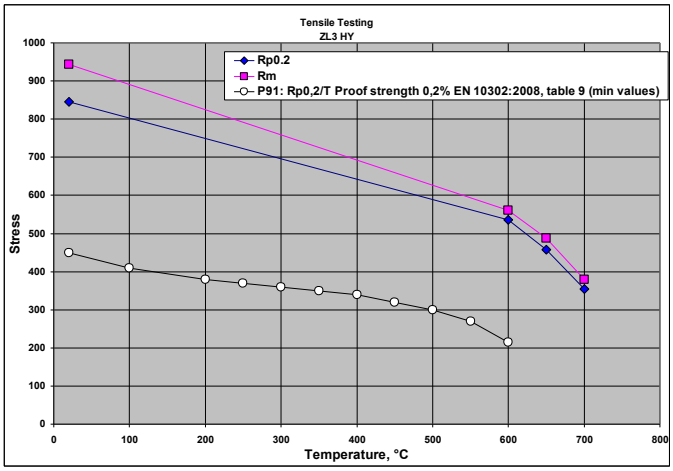

(a)

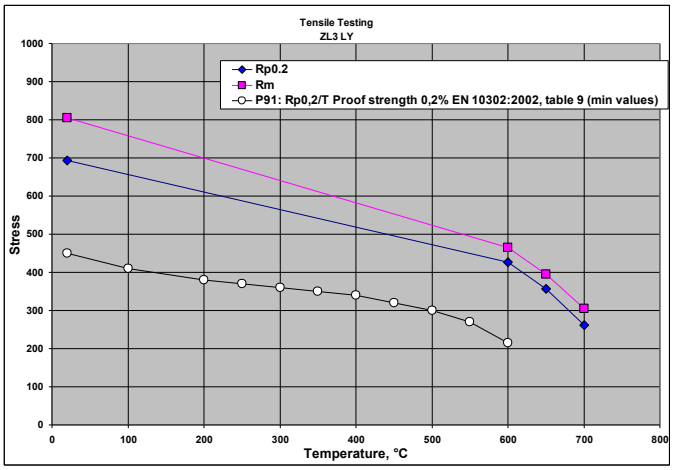

(b)

Figure 3-4. *Tensile testing at elevated temperatures for two heat treatment varieties of ZL3 alloy (a) ZL3 HY and (b) ZL3 LY.*

3.3.3 Long term creep testing

Figure 3-5 shows the creep rupture strength versus fracture time curves at 650°C for Z3 and Z4 steels in comparison with the benchmark ASTM grade P91 (9% Cr–1% Mo–0.2% V–0.05% Nb) and ASTM grade P92 (9% Cr–0.5% Mo–1.8% W–0.2% V–0.05% Nb), two of the most widely used 9-12% Cr steels today. After more than 11,000 hours the creep strength of the CrTaN-strengthened Z4 steel is better than that of P91 and close to that of P92, and the creep property of the CrNbN-strengthened Z3 steel is comparable with that of P91.

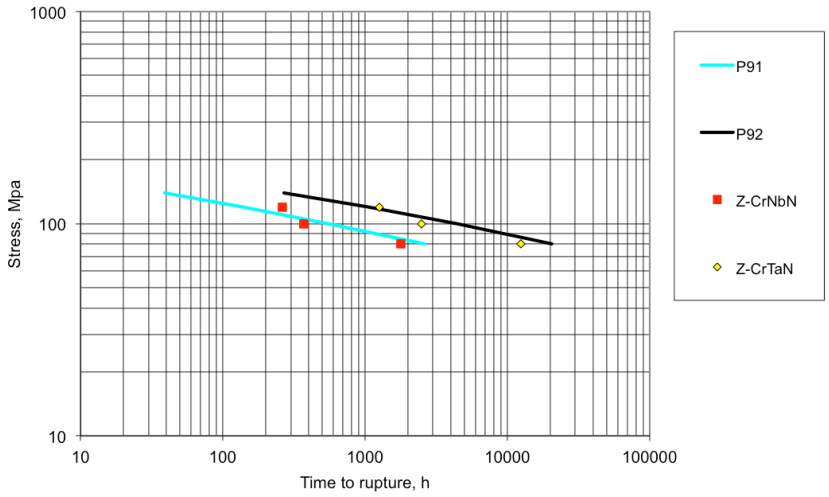

Figure 3-5. *Creep rupture results at 650°C for the new Z-phase strengthened steels, Z4 CrTaN-containing and Z3 CrNbN-containing, in comparison with two benchmark commercial steels.*

Creep testing at 625°C of ZL1 (1050°C/1h+700°C/7h), ZL2 (1050°C/1h +700°C/7h), ZL3 LY (1150°C/1h+650°C/6h+740°C/6h) and ZL3 HY (1150°C/1h+650°C/6h+700°C/6h) has been started. The testing of ZL3 at certain stress conditions is still under progress (the data points with an arrow in ***Figure 3-6***). The creep rupture results, obtained so far, are shown in ***Figure 3-6***. All the ZL series steels exhibit a creep strength between Z3 and Z4.

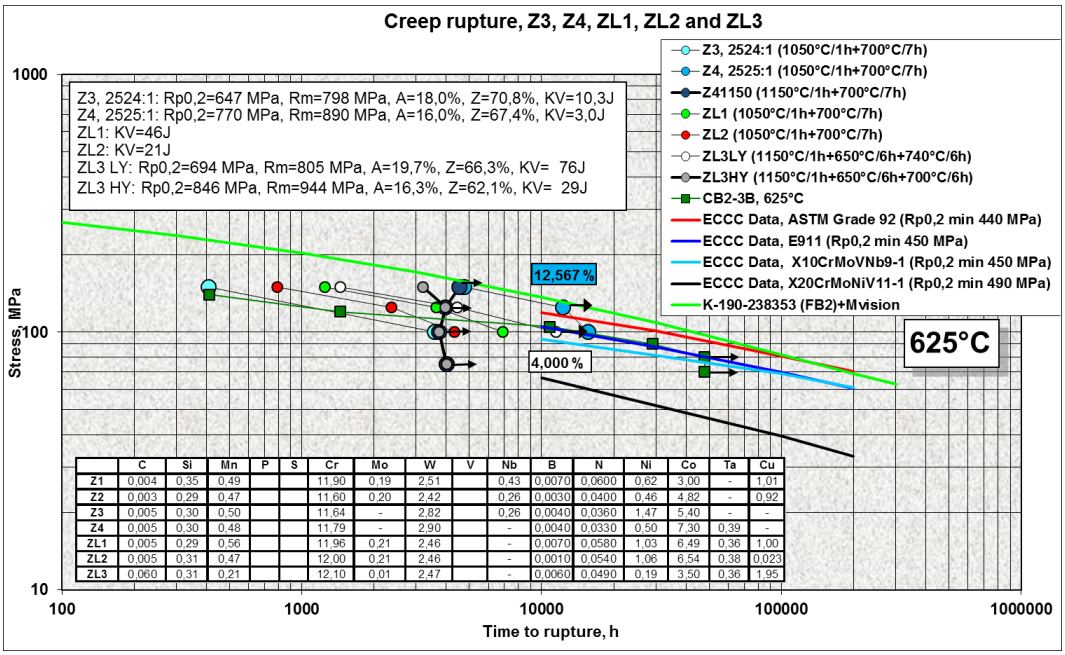

	C	Si	Mn	P	S	Cr	Mo	W	V	Nb	B	N	Ni	Co	Ta	Cu
Z1	0,004	0,35	0,49			11,90	0,19	2,51		0,43	0,0070	0,0600	0,62	3,00	-	1,01
Z2	0,003	0,29	0,47			11,60	0,20	2,42		0,26	0,0030	0,0400	0,46	4,82	-	0,92
Z3	0,005	0,30	0,50			11,64	-	2,82		0,26	0,0040	0,0360	1,47	5,40	-	-
Z4	0,005	0,30	0,48			11,79	-	2,90		-	0,0040	0,0330	0,50	7,30	0,39	-
ZL1	0,005	0,29	0,56			11,96	0,21	2,46		-	0,0070	0,0580	1,03	6,49	0,36	1,00
ZL2	0,005	0,31	0,47			12,00	0,21	2,46		-	0,0010	0,0540	1,06	6,54	0,38	0,023
ZL3	0,060	0,31	0,21			12,10	0,01	2,47		-	0,0060	0,0490	0,19	3,50	0,36	1,95

Figure 3-6. *Creep rupture results at 625°C for the new ZL series. Creep testing that is under progress is indicated by with an arrow on the data points.*

3.4 Microstructure investigation

Microstructure dictates properties of materials. For this new generation of steels, a systematic investigation of their microstructure, and microstructure evolution at high temperatures is essential to understand their mechanical behaviour. And in turn the understanding gained on microstructure facilitates further alloy design optimization, which can lead to improved mechanical properties. Advanced microstructural analysis techniques, such as scanning electron microscopy (SEM), transmission electron microscopy (TEM), and atom probe tomography (APT) were used.

This section is organized like this: first we show the results of the microstructure analysis methodological development performed within this project: sample preparation optimization and high resolution backscattered electron imaging in SEM; then we present the detailed microstructure study results of different test alloys.

3.4.1 Sample preparation method optimization for electron microscopy

Several sample preparation methods can be employed for microstructure investigation of steels. Each method might introduce some artefacts and it is very important to identify these artefacts for a better understanding of microstructure. We have employed three different methods of sample preparation: mechanical polishing, electropolishing, and ion milling.

Mechanical polishing is the most basic method that one employs to prepare samples for microstructural investigations. For electropolishing, the specimen needs to undergo first mechanical polishing and then chemical polishing. Using ion milling and polishing method for sample preparation is the most time consuming method among aforementioned methods. Different sample preparation methods give very different starting point for microstructure analysis. ***Figures 3-7 (a), (b), and (c)*** show micrographs obtained from ZL3 aged for 5500 hours at 650° prepared by mechanical polishing, electropolishing, and ion polishing, respectively.

As can be seen in ***Figure 3-7 (a)***, for mechanical polishing there are some small particle-like features with black contrast highlighted by black arrows. However, these areas do not exist in the specimens prepared by other methods. Therefore, this black contrast is likely to be an artefact of mechanical sample preparation. In addition by using this method, it is not possible to totally remove the scratches, which is obvious in the micrograph.

Electropolishing can yield very thin areas on a specimen (< 100 nm) that can be used in TEM. However, with this method, Cu particles tend to dissolve in the electrolyte during sample preparation, and leave holes in the sample. In addition, at certain positions quite a large volume of precipitates that does not belong to the volume of the thin film, lie on the film, like the agglomeration of $M_{23}C_6$ particles in ***Figure 3-7 (b)***. This will lead to overestimation of the

$M_{23}C_6$ volume fraction because the total volume is calculated based on the thickness of the thin film.

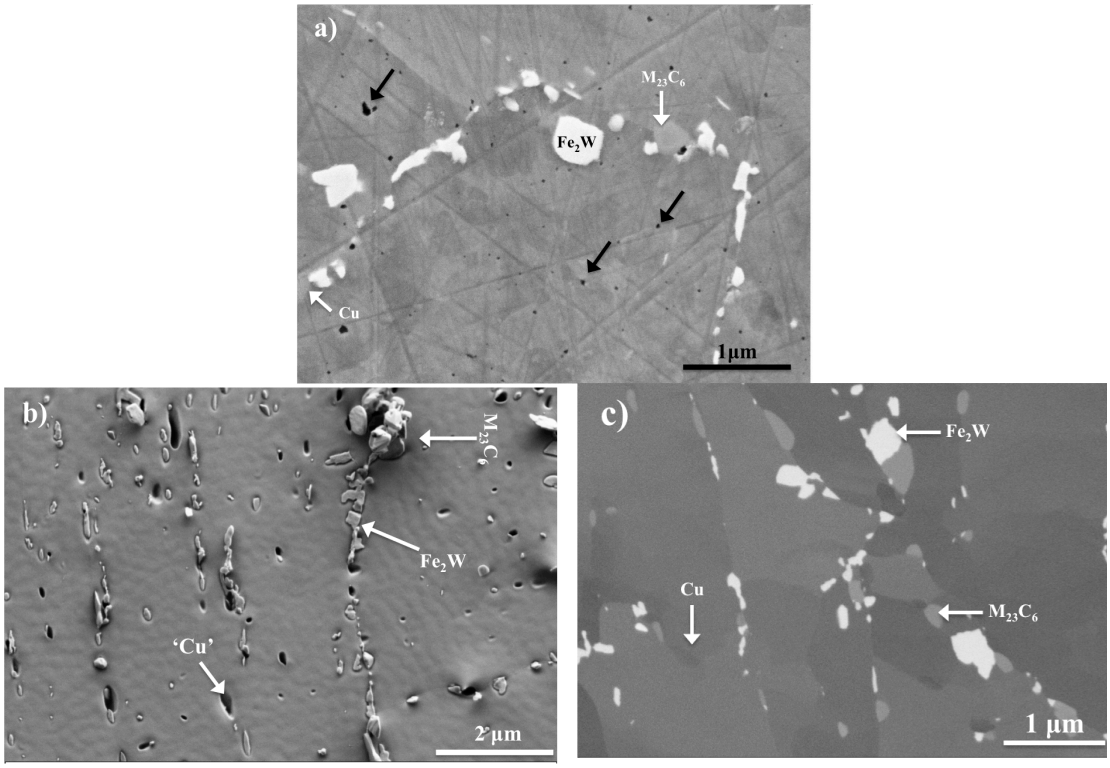

Figure 3-7. *SEM micrographs of ZL3 after 5,500 hours aging (a) secondary electron image of mechanically polished specimen,(black arrows highlight the areas with black contrast) (b) secondary electron image of electropolished specimen, and (c) electron backscattered image of ion milled specimen.*

The ion milling and polishing method also provides the possibility of yielding very thin electron transparent specimens. However, compared to electropolishing it has the advantage of leaving Cu particles intact for TEM analysis. This time-consuming method provides better specimens for microstructure analysis with fewer artefacts. However due to a wavy surface as a result of prolonged ion milling, the quality of secondary electron micrographs is not good.

3.4.2 High resolution backscattered SEM imaging by EsB

In this project we used EsB (Energy and angle Selective Backscattered) detector in a SEM to obtain high-resolution backscattered electron images that can clearly reveal precipitates of nanometre size. Secondary electrons are often used to form images in a SEM because they provide the highest spatial resolution. These images mainly carry topographic information. Backscattered electrons, on the other hand, carry chemical information, and can form images with so-called atomic number contrast, where areas with higher

atomic number appear brighter. However, the resolution of the ordinary backscattered images is typically limited to around 0.5 micrometres. When the SEM is operated at a rather low accelerating voltage, the low energy loss electrons that carry chemical information from the very surface (a few nanometres) of the material, can be collected by the EsB detector installed inside the electron column. This allows a SEM micrograph with chemical information and a resolution as high as 10-20 nm (see ***Figure 3-8***).

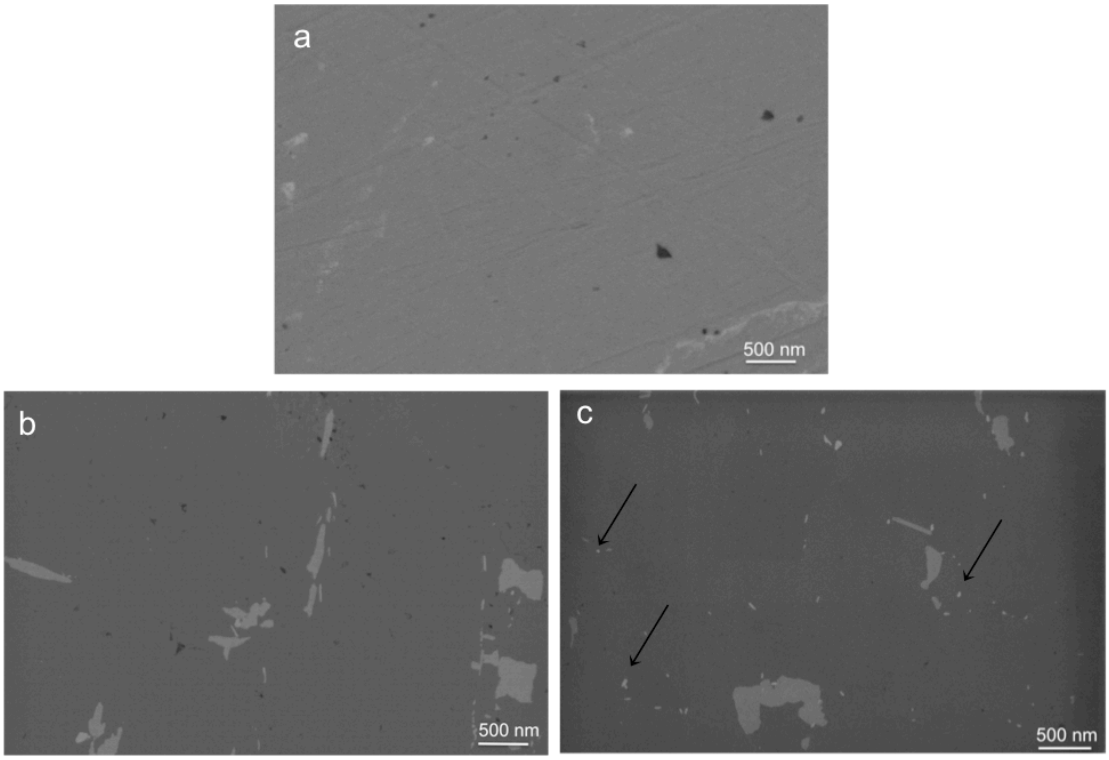

Figure 3-8. *SEM backscattered electron images taken by using an EsB detector. Z4 is aged for (a) 24 hours (b) 3000 hours and (c) 10,000 hours. After 24 hours there are very few precipitates (the white areas), and they do not have a clear boundary to the matrix. After 3,000 hours the boundary is very clear. After 10,000 hours, there are some small precipitates with brighter contrast (arrowed).*

3.4.3 Boundaries in steels by EBSD analysis

We used EBSD to reveal quantitative crystallographic information, such as orientation relationship, and percentage of high angle boundaries.

EBSD analyses were performed on the benchmark ASTM grade P92 (1070°C/2h + 780°C/2h), Z4 (1050°C/1h or 1150°C/1h followed by 720°C/6h) and a new Japanese steel BH (1050°C + 780°C). Grain boundary

maps are shown in ***Figure 3-9***. A big difference between the steels was found in terms of crystallographic orientation.

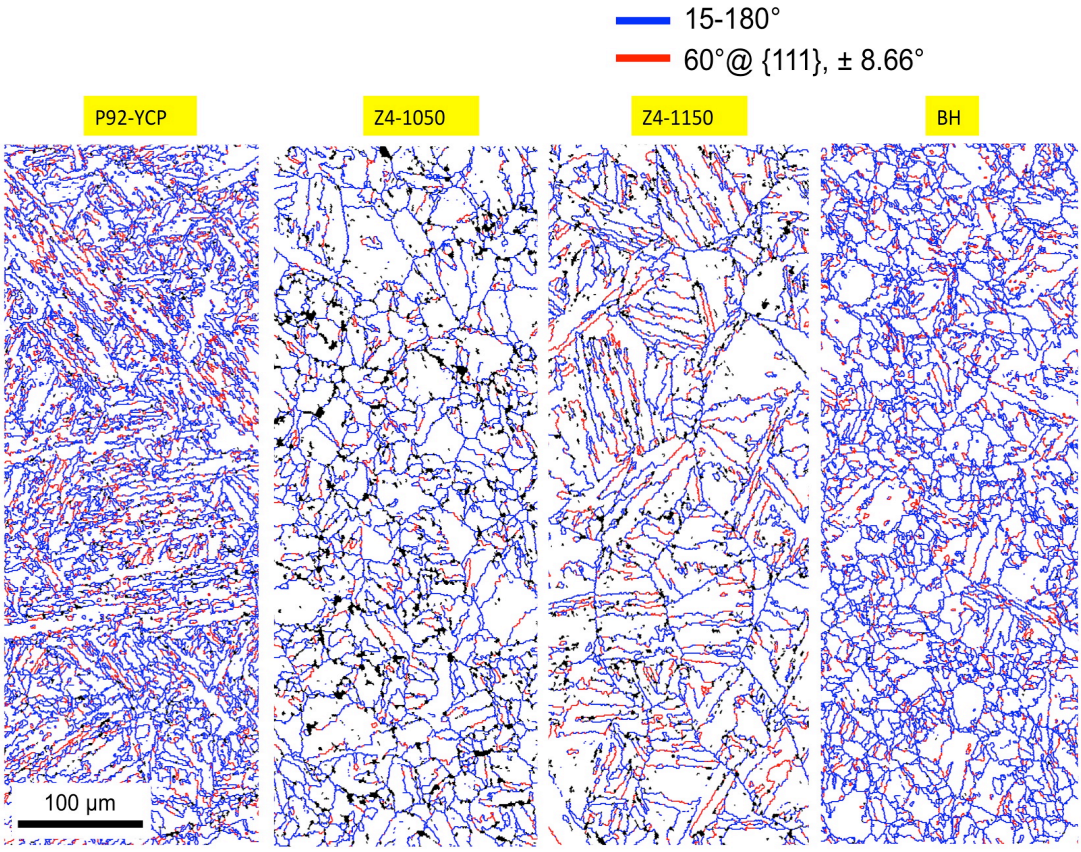

Figure 3-9. *EBSD grain boundary maps for P92 (1070°C/2h + 780°C/2h), Z4 (1050°C/1h + 720°C/6h), Z4 (1150°C/1h + 720°C/6h), and a new Japanese steel BH (1050°C + 780°C). The blue lines indicate high angle (15-180°) boundaries and red lines indicate special boundaries.*

Quantification of the grains and boundaries were carried out. The results are summarized in ***Table 3-6***. The main findings are:

- P92: Fraction of low angle grain boundary (LAGB) and high angle grain boundary (HAGB) and special boundaries follows average.
- Z4 (1050°C/1h + 720°C/6h): Highest fraction of LAGB. Lowest fraction of HAGB.
- Z4 (1150°C/1h + 720°C/6h): Fraction of LAGB and HAGB follow average.
- BH: Lowest fraction of LAGB. Highest fraction of HAGB.

P92 has large prior austenite grains (PAGs) with many small blocks, and very varying orientation. The projection on the pole figure is very scattered,

indicating that the orientation relationship (OR) is not followed exactly. Almost all variants are found in the PAGs.

Z4 (1050°C/1h + 720°C/6h) has small PAGs, which contain very few blocks. Shapes of PAGs are irregular, and there is no straightforward identification of PAG. Only a few variants per PAG, and many points inside of a PAG fall out of Kurdjumov-Sachs or Nishiyama-Wasserman (KS/NW) orientation relationship, which leads to a blurry projection in the pole figure.

In Z4 (1150°C/1h + 720°C/6h), PAG, blocks, and packets appear as textbook examples; they are readily identifiable. Each PAG contains many blocks and almost a full variant selection. There is a large misorientation within each block, which indicates a significant lath structure. Many twins were found in the PAGs, and they are visible from pole figures.

BH has very small PAGs with very few blocks, and a few variants. Shapes of PAGs are irregular. PAGs are very difficult to identify sometimes. Often twins separate these small PAGs. There are a few large PAGs, which contain many blocks and a full variant selection. BH contains a large number of high angle grain boundaries.

Table 3-6. *Quantitative of EBSD results.*

	P92 YCP	Z4 1050	Z4 1150	BH
PAG				
Number of variants (out of 24)	≈24	≈12	≈22	≈12
Area (AA)	22402	1804	18632	4179
Eq diameter (AA)	169	48	154	73
Area (NA)	18816	1366	12283	2110
Eq diameters (NA)	155	41.7	125	52
Blocks				
Blocks per PAG	337	8.7	57	14.6
Area (AA)	279	633	1416	662
Eq diameter (AA)	18.8	28.4	42.5	29.0
Area (NA)	69	157	217	145
Eq diameter (NA)	9.4	14.1	16.6	13.6
Major length (AA)	15.5	20.5	38.7	22.8
Minor length (AA)	4.8	7.7	11.6	7.6
Aspect ratio (AA)	0.35	0.39	0.31	0.35

All values are average values, either area average (AA) or number average (NA)

Areas are in μm², diameters in μm, and lengths are in μm.

3.4.4 Primary precipitates

SEM was used to provide an overview of primary precipitates. Two types of primary precipitates were observed: BN particles (> 1 micrometre) with dark

contrast and irregular morphology, and big TaC/NbC (> 0.5 micrometre) with bright contrast and spherical morphology. The former exists only in the ZL3 steel, and the latter exists in all test steels. The typical morphology and corresponding EDX spectra of these precipitates are shown in ***Figure 3-10***.

Boron is known to retard coarsening of $M_{23}C_6$ precipitates [13]. Nitrogen is supposed to form nano-sized (carbo)nitrides and Z-phase that efficiently strengthen the steel. Forming BN particles consumes the beneficial elements B and N. The BN particles themselves are too large to contribute to strengthening. The presence of BN in ZL3 indicates that the chemical composition of the steel needs further fine-tuning.

Similarly, TaC/NbC particles consume Ta/Nb, which is expected to contribute to Z-phase formation. However, TaC/NbC particles can, to some extent, lock PAGBs and avoid extensive grain coarsening during the austenitization process.

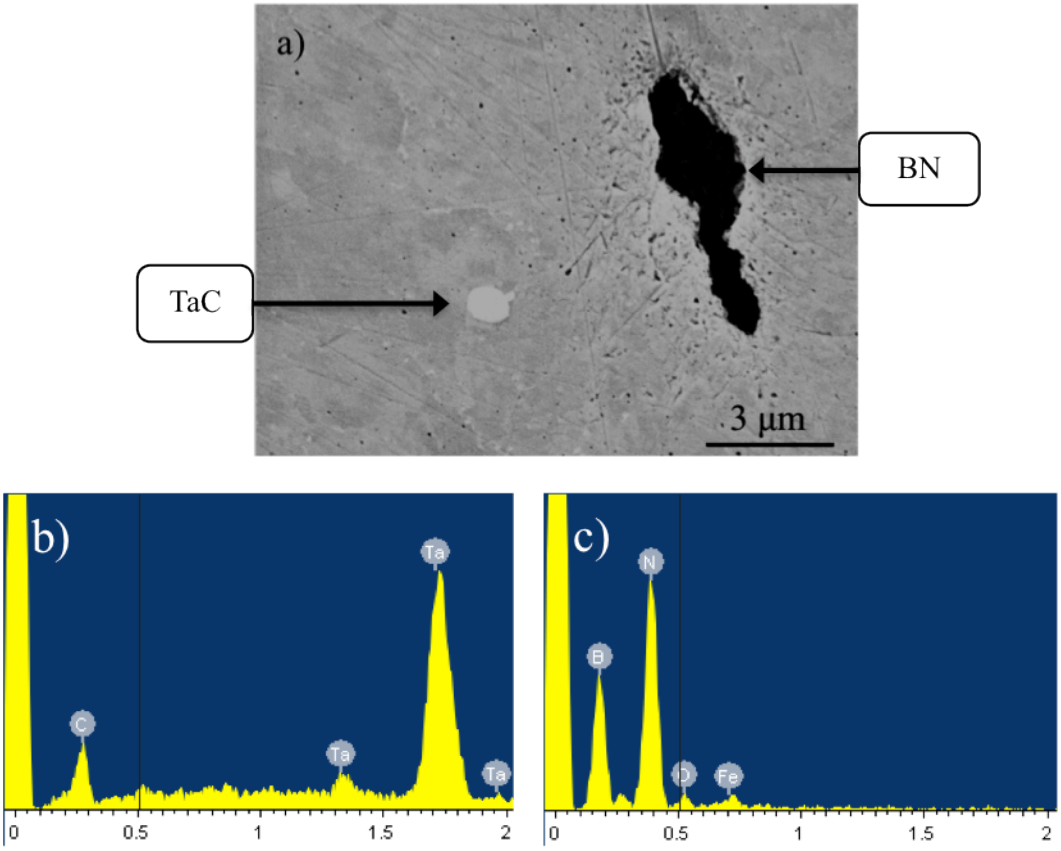

Figure 3-10. *Primary precipitates in ZL3. (a) SEM secondary electron micrograph showing TaC and BN. EDS spectra for (b) the TaC and(c) the BN.*

3.4.5 Secondary precipitate microstructure evolution in Z3 and Z4

Secondary precipitates are the key player in terms of strengthening 9-12%Cr steels at elevated temperatures. Investigation of their evolution is the essential part of microstructure analysis.

3.4.5.1 Microchemistry of the steel matrix by APT - overall precipitation reactions

The changes in chemical composition of the matrix can give us some indication of the overall precipitation reactions in the material. The concentration of different elements in the matrix of Z4 aged for 24, 1,005 and 10,000 hours was measured by APT. The results are summarized in ***Table 3-7***. It showed that most Ta and N had precipitated out of the matrix after 24 h. On the other hand, the W content keeps decreasing after 24 hours until 1,005 hours. From 1,005 hours to 10,000 hours, only a very slight decrease of W was observed. This indicates that most Laves phase (Fe_2W) had precipitated within ~1,000 hours.

Table 3-7*. Chemical composition evolution of matrix of Z4 (in* ***atomic*** *percent).*

	Fe	Ni	Co	Cr	W	Nb	Ta	C	B	N	Si	Mn
Z4 24h	Bal.	0.67	7.40	12.65	0.63	-	0.007	0.003	0.002	0.006	0.59	0.51
Z4 1005h	Bal.	0.57	7.47	12.54	0.24		0	0	0	0	0.61	0.49
Z4 10000h	Bal.	0.8	7.45	12.39	0.2		0	0	0	0	0.63	0.53

3.4.5.2 Fine Z-phase precipitates by APT

Very fine (a few nanometre) and dense Z-phase precipitates were formed in test steels Z4 and Z3 after just 24 hours. They are too small to be readily imaged by TEM. However, APT can provide both morphology and chemical composition of these small precipitates.

In the Z4 steel after 24 hours of aging, only small precipitates rich in Cr, Fe, Ta, Co, N and W were observed. The precipitates can be visualized by the atom reconstruction (box size: 85 × 85 × 60 nm^3) in ***Figure 3-11 (a)***, where TaN ions are displayed as dots. Ta-atom enriched areas show the location of the precipitates. These precipitates are blade-like, with typical thickness ~1 nm, and length 5-15 nm. In this figure, the arrowed precipitate aligns so that

its thinnest plane is roughly parallel to the projection plane, and it gives the reader an idea of the thickness. The precipitates are in a large number; their number density is ~10^{23} m^{-3}. The chemical composition varies for individual precipitates depending on the size.

Figure 3-11 (b) shows the NbN- molecular ion map for Z3 test steel. These molecular ions in Z3 stem from Z-phase precipitates, rod-like and 10-40 nanometre in size. Note the large difference in reconstructed volume between the figure (a) and (b).

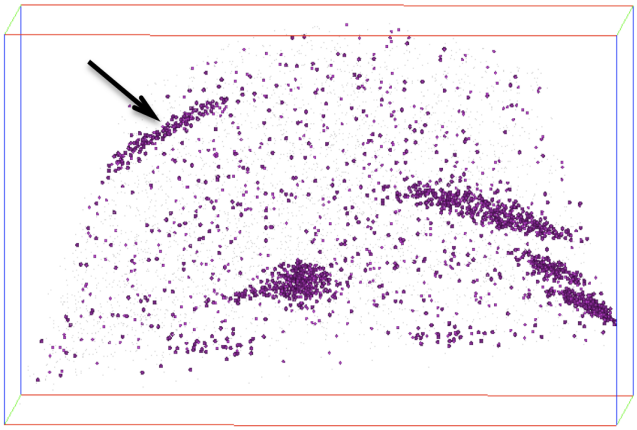

(a) box size: 85 × 85 × 60 nm^3

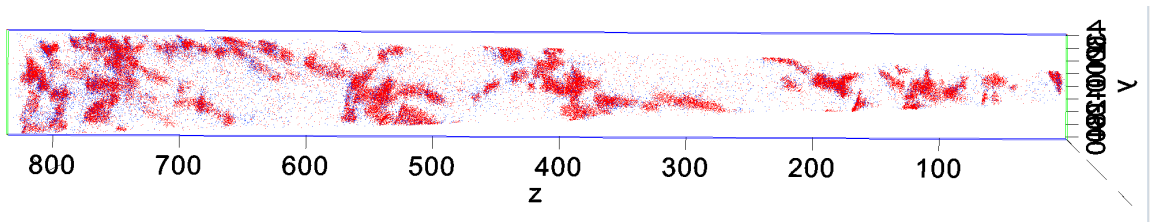

(b) box size: 80 x 80 x 830 nm^3

Figure 3-11. *Reconstruction of APT datasets obtained from the (a) Z4, and (b) Z3 sample heat-treated at 1150°C 1h + 650°C 24h. The purple and red dots represent TaN- and NbN- molecular ions, respectively. Note the large difference in reconstructed volume in the figures.*

After 1005 hours aging, the Z-phase precipitates have coarsened to some extent, compared to after 24 hours aging. A couple of APT samples, with a total volume of around 10^6 nm^3, were analysed for each material with different aging times. For the Z3 steel only a part of a big Nb-containing Z-phase precipitate together with two small ones in the immediate vicinity to it was observed. The part of the precipitate detected had a size of ~ 60 x 20 x 10 nm^3. For Z4, one big (50 nm) and several small Z-phase precipitates were observed. The precipitates had become spherical or rod-like in shape. Their typical size was 5-15 nm. For Z4, the number density of the precipitates were ~ 2 × 10^{22} m^{-3}, based on the APT results.

The chemical composition of the Nb- and Ta-containing Z-phase particles is listed in ***Table 3-8***. For the Nb-containing Z-phase, considering experimental errors, the ratio of Cr:Nb(+Ta+V):N is reasonably close to 1:1:1. Although not given in the nominal composition, small amounts of V and Ta were detected, which are believed to be incorporated impurity from material preparation. Some Fe, Ni, Co, W, Mn, together with B and C, were found in the precipitate as well.

On the other hand for the Ta-containing Z-phase, it is noticeable that the Ta concentration is remarkably less than 33%; even after counting in Nb and V, the concentration only makes up to 27%. On the other hand, Cr concentration is more than 33%, reaching 36%. The concentration of W, Mn and V are close to those in the Z3 steel, while Fe, Ni, Co, C and B concentration are somewhat lower compared to the Z3 steel.

Table 3-8. *Chemical composition evolution of Z phase (in* ***atomic*** *percent).*

	Fe	Ni	Co	Cr	W	Nb	Ta	V	C	B	N	Mn
Z4 1005h	3.08	0.09	0.13	36.20	1.26	1.35	23.76	1.15	0.32	0.14	32.32	0.20
Z4 10000h	1.31	0.08	0.06	35.37	0.33	1.39	25.5	1.18	0.56	0.087	33.9	0.18
Z3 1005h	3.62	0.05	0.08	29.19	0.94	31	-	1.14	1.38	0.2	32.2	0.16
Z3 10000h	3.66	0.015	0.16	34.88	1.29	29.29	-	0.37	0.66	0.13	29.4	0.11

It was found that C was distributed rather evenly in the entire particle. On the other hand, B was enriched at the interface between the precipitate and the matrix (***Figure 3-12***).

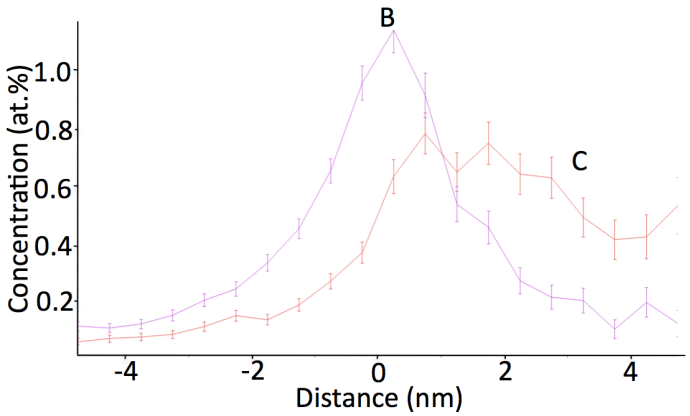

Figure 3-12. *Proxigram analysis showing quantitative B and C concentration profiles across a large CrNbN-particle/matrix interface in* the *CrNbN-based steel.*

3.4.5.3 Quantitative analysis of secondary precipitates based on SEM

Quantitative image analysis was performed on SEM micrographs of the Z4 steel aged for the 3,000 hours and 10,000 hours. Examples of the micrographs are shown in ***Figure 3-8***. More than 4,000 precipitates in total were analysed. The average area fraction of the precipitates was 2.25 ± 0.67 % and 2.85 ± 0.69 % for the 3,000 hours and 10,000 hours sample, respectively.

Size distribution histograms are shown in ***Figure 3-13***. In both cases, precipitates with small sizes (less than ~140 nm in equivalent diameter) are predominant in terms of numbers. They also contribute to most of the area fraction. For the 3,000 hours sample the accumulated area for these precipitates reaches 19% out of the total area of precipitates. For the 10,000 hours sample this value is lower, ~14%. On the other hand, the number of very small precipitates (<30 nm) increases dramatically from 3,000 hours to 10,000 hours. Therefore, the decrease in the accumulated area for the small precipitates is solely due the fact that the number of large precipitates (>400 nm) in the 10,000-hour sample increases. These precipitates are mainly coarse Laves phase.

The APT results of the matrix chemical composition (see ***Table 3-7***) predict only a rather slight increase (less than 5%) in the volume percentage of Laves phase. However, an apparent increase in area percentage for precipitates of more than 25% is obtained by image analysis. This difference is too large to be justified by the process of converting 2-D measurement to 3-D information. In fact, that very small Z-phase precipitates grew larger and became detectable by SEM accounts mainly for the significant increase of the area occupied by precipitates. This is proved by the following TEM and APT results on Z-phase precipitates.

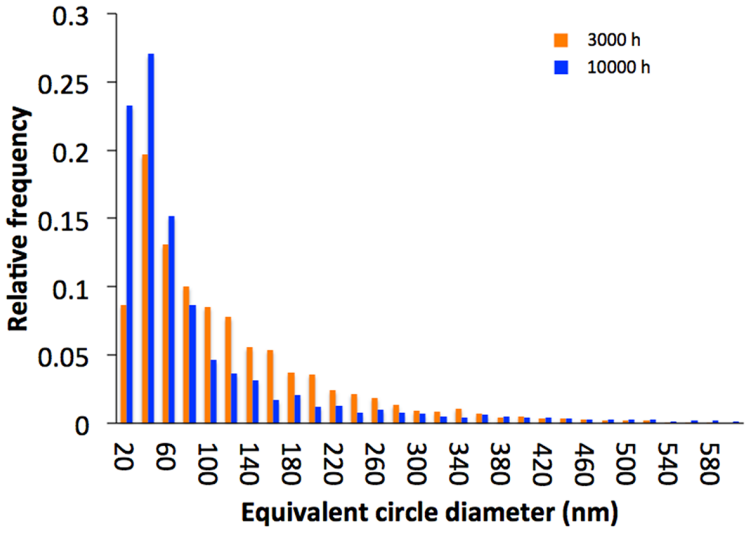

Figure 3-13. *Precipitate size distribution for the sample aged for (a) 3,000 hours, and (b) 10,000 hours.*

3.4.5.4 TEM investigation

Further analysis using TEM/EDX showed that the visible precipitates in the Z4 24 hours sample contain mainly W (***Figure 3-14***). Ta-containing precipitates are clearly visible after 10,000 hours. Mainly forming along the lath boundaries, they are enriched in Cr as well (***Figure 3-15***). The results suggest that a large portion of the "newly-formed" very small precipitates in the 10,000-hour sample observed in the SEM is Z-phase precipitates, which coarsened with time, and thus became visible in the SEM.

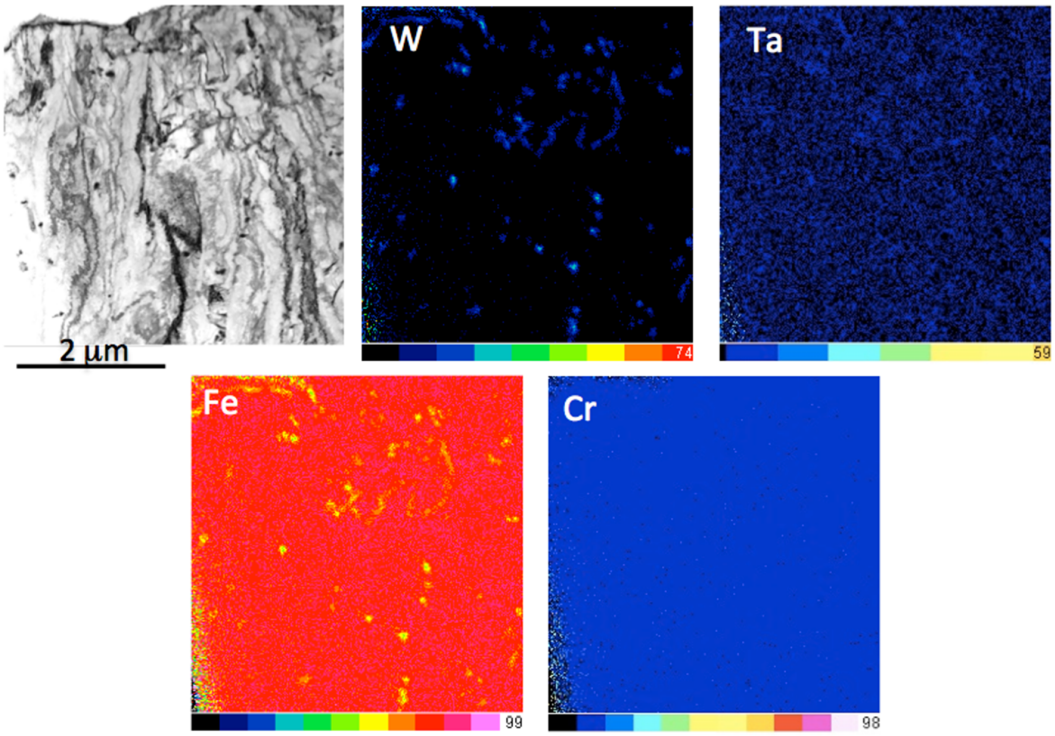

Figure 3-14. *TEM/EDX mapping of the precipitates in the Z4 steel aged at 650°C for 24 hours. (a) bright field image. Elemental maps for (b) W, (c) Ta, (d) Fe, and (e) Cr. Only Laves phase particles are visible.*

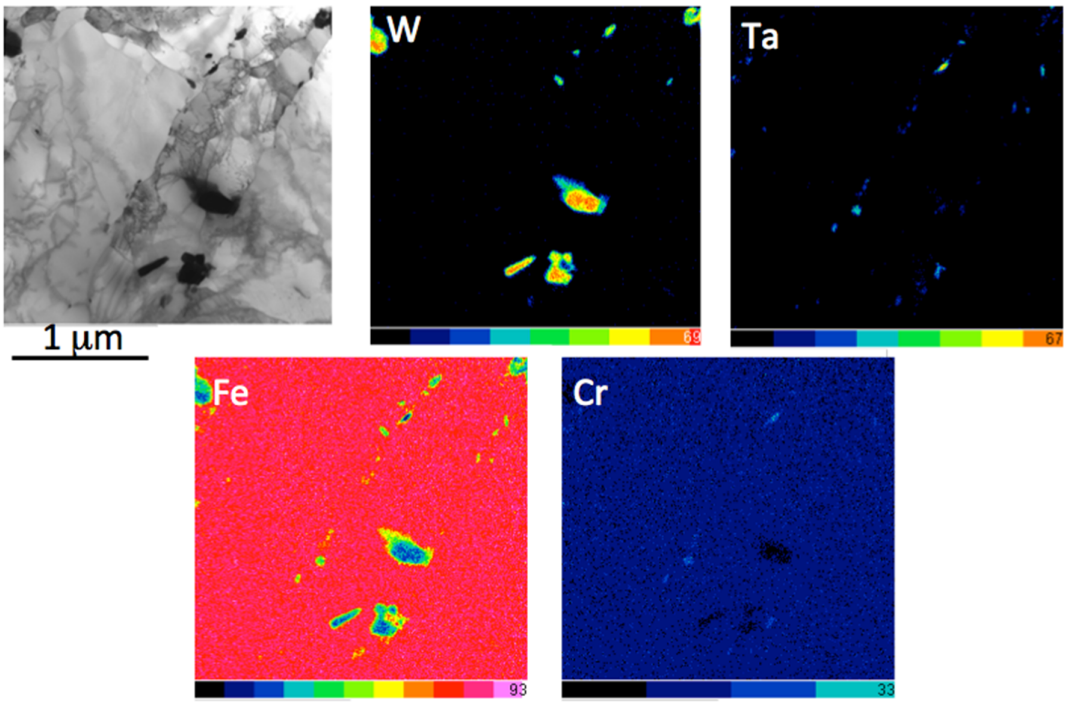

Figure 3-15. *TEM/EDX mapping of the precipitates in the Z4 steel aged at 650°C for 10,000 hours. (a) bright field image. Elemental maps for (b) W, (c) Ta, (d) Fe, and (e) Cr. Both Laves phase (Fe_2W) and small Z-phase (CrTaN) particles are visible.*

3.4.5.5 Laves phase in Z3 and Z4

APT samples containing Laves phase particles were specially prepared either by controlled back-electropolishing (iteration between polishing and checking in a SEM) or by focused ion beam milling. Laves phase formed after different aging times were analysed and the results are presented in ***Table 3-9***. With time there is a continuous increase in Fe and W concentrations, and a decrease in Cr concentration. Some N was found in the Laves phase after 1005 hours. B and C concentrations depend on the relative position of the analysed volume, since they tend to be enriched at phase boundaries.

Table 3-9. *Chemical composition evolution of Laves phase in Z3 and Z4 (in* ***atomic*** *percent).*

	Fe	W	N	Ni	Co	Cr	Nb	Ta	C	B	P	Si	Mn
Z3 24h	42.73	26.61	0.2	1.17	3.72	17.37	2.11	0.01	0.24	0.87	0.12	3.49	0.81
Z3 1005h	45.04	29.33	0.047	0.63	3.35	14.97	1.63	0.02	0.03	0.12	0.04	3.60	0.59
Z3 3000h	44.49	30.09	-	0.22	3.49	15.75	1.17	-	0.29	0.46	0.1	2.94	0.62
Z3 10000h	45.79	29.7		0.61	3.40	13.83	1.86	-	-	0.018	0.04	3.88	0.56
Z4 1005h	41.00	30.22	0.22	0.28	4.66	17.00	0.02	1.24	0.04	0.37	0.03	2.79	0.67
Z4 3000h	42.33	31.65		0.42	4.72	16.43		0.63	0.154	0.144	0.032	2.84	0.66
Z-4 10000h	44.27	29.71		0.54	4.7	16.09		0.72	0.08	0.10	0.02	3.1	0.68

3.4.6 Microstructure of ZL Series

Steels Z3 and Z4 had very poor impact toughness in Charpy V-notch testing, showing on average only 3 J absorbed energy. By adding less than 2 at.% Cu (steel ZL1), the impact energy absorption was remarkably improved, reaching 46.3 J. For the second stage of the project much effort was spent to understand the effect of Cu.

3.4.6.1 The effects of Cu – Z4 vs. ZL1

SEM

After tempering both Z4 and ZL1 exhibit a martensitic/ferritic microstructure, containing prior austenite grains and laths. SEM backscattered electron micrographs (***Figure 3-16 (a) and (c)***) show clearly the prior austenite grain boundaries, which give bright contrast in the images. It is worth noticing that both samples were polished but without any etching. The contrast in

backscattered electron imaging arises mainly from the difference in atomic number: bright contrast indicating regions with heavier atoms. Thus the prior austenite boundaries are decorated by some heavy elements. Further EDX analysis revealed W enrichment in the regions.

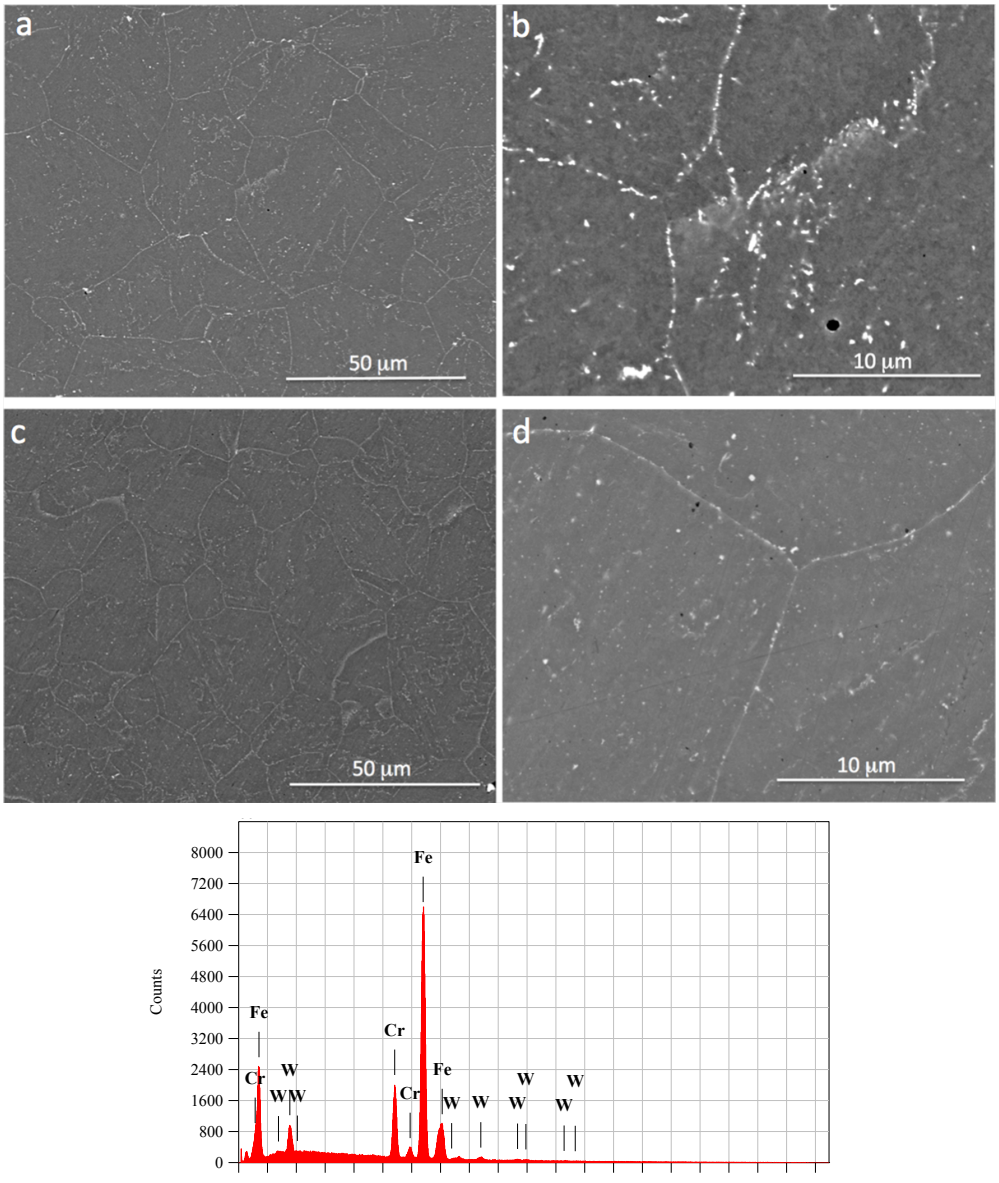

***Figure 3-16**. SEM backscattered electron micrographs of (a) and (b) steel Z4; (c) and (d) steel ZL1 in the as tempered condition. Laves phase precipitates (bright particles) decorate prior austenite grain boundaries in both steels. An EDX spectrum of the bright particles indicates that they are Laves phase.*

Images with higher magnifications (***Figure 3-16 (b)*** and ***(d)***) show more detail in these regions. There are W-enriched Laves phase precipitates ($Fe_2(W,Mo)$) forming along prior austenite grain boundaries and also inside

the grains. Overall in steel Z4 (***Figure 3-16 (b)***) Laves phase precipitates are larger in size but fewer in number as compared to steel ZL1. However, in steel ZL1 (***Figure 3-16 (d)***) precipitates on the grain boundary regions are much fewer; on the other hand there is a large number of very small precipitates inside the grains. They are so small that they only give rather faint grey contrast in the image. We believe that the preferential precipitation of Laves phase particles along prior austenite grain boundaries are responsible for the poor impact strength for steel Z4. Cu (~1wt%) and/or Mo addition in steel ZL1 can modify Laves phase nucleation and distribution.

Two different types of Laves phase morphology can be identified in steel ZL1 aged for 300 h (***Figure 3-17 (a)***): the "normal" equiaxed (indicated by thick arrows), which is the only type observed in the steel Z4, and the elongated rod-shaped (indicated by thin arrows), which are basically absent in the steel Z4. In steel Z4 aged for 1,000 hours (***Figure 3-17 (b)***) largely only the equiaxed type of morphology was observed, while in ZL1 aged for 1,000 hours there are a large number of elongated rod-shaped Laves (***Figure. 3-17 (c)***). Interestingly, they are aligned in certain directions, which suggests that there is a certain preferential crystallographic orientation relationship between these Laves-phase precipitates and the steel matrix.

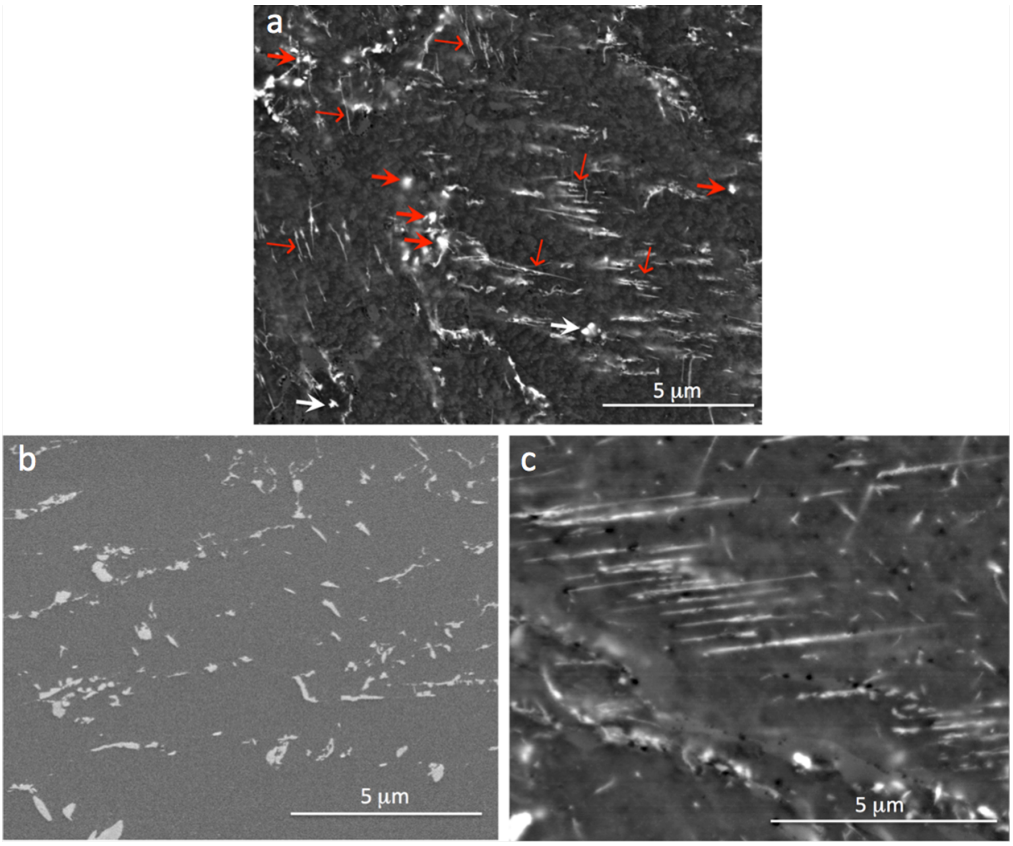

Figure 3-17. *SEM backscattered electron micrographs of (a) steel ZL1 aged for 300 h; two types of morphology: equiaxed (indicated by thick arrows) and elongated (indicated by thin arrows). (b) Steel Z4 aged for 1,000 h, mainly equiaxed type morphology. (c) ZL1 aged for 1,000 h, a large number of elongated type of Laves particle.*

The morphology difference is also believed to be related to the Cu addition. In order to understand the process of Laves phase precipitation, Cu behaviour, and if there is any connection between Cu and Laves particles, for instance Cu partitioning to Laves or segregation of Cu to the interface between Laves phase and the steel matrix, APT analysis was performed.

Laves phase particle

In order to understand if Cu affects the morphology of Laves phase by partitioning to the precipitates, we performed APT analysis specifically of elongated Laves phase particles in steel ZL1 aged for 300 hours. APT specimens with a part of an elongated Laves particle on the very tip were prepared by using the in-situ lift out technique. This part of Laves phase particle comes originally from the middle of a rod.

Figure 3-18 (a) is atom map for W (dark red dots) and Fe (magenta dots) from an APT reconstruction of a volume that contains part of an elongated Laves phase particle on top. ***Figure 3-18 (b)*** shows the part of the mass spectrum that contains information for Cu^{1+}. Note, firstly only atoms from the Laves phase are included in the spectrum. Secondly, the isotope abundance of Cu is 69% at ^{63}Cu, and 31% at ^{65}Cu (the height of the dashed red line corresponds to the abundance of the two isotopes). Thirdly, the peaks of $^{65}Cu^{1+}$ and $^{181}Ta^{14}N^{3+}$ are located very close in the spectrum at around 65 Da. No ion was detected for the major Cu peak at 63 Da, therefore, we can conclude that there is virtually no Cu in this volume of Laves phase and that all ions recorded at 65 Da are TaN^{3+} ions.

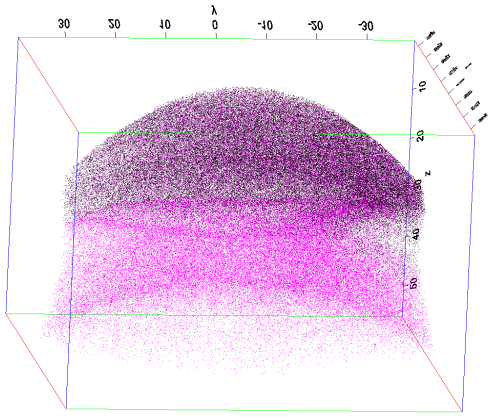

(a)

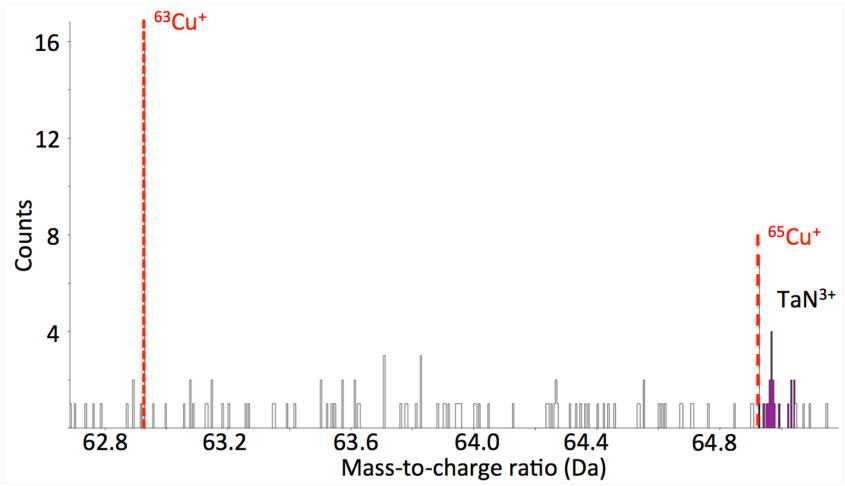

(b)

Figure 3-18. *(a) Reconstruction of an APT dataset obtained from steel ZL1 aged for 300 h. It contains a part of an elongated Laves phase on the top. The dark red and magenta dots represent W and Fe atoms, respectively. For visual clarity only 5% of Fe and 30% of W atoms are shown. The box size is: 80 × 80 × 56 nm^3. (b) Part of the mass spectrum of the Laves phase particle only. The dashed red lines indicate the position of Cu isotopes in the spectrum. Their height corresponds to the abundance of the two isotopes. No Cu was found in the Laves phase.*

Chemical composition of the elongated Laves phase was obtained using APT. The results are displayed in ***Table 3-10***. It has the basic chemical formula of $(Fe,Cr,Co)_2(W,Mo,Si)$. This volume of Laves phase contains no Cu.

Table 3-10. *APT results from an elongated Laves-phase particle in steel ZL1 aged for 300 h (in* ***atomic*** *percent).*

Fe	W	N	Ni	Co	Cr	Ta	C	B	Si	Mn	Mo	Cu
43.0	26.2	0.34	0.52	4.0	18.6	0.55	0.27	0.34	2.68	0.75	2.8	-

Chemical composition of Cu-rich particles

The chemical composition of a Cu-rich particle was acquired using APT. The results are displayed in ***Table 3-11***. It contains almost pure Cu (> 98%), with small amount of Mn and Ni, and trace amount of Fe, Co and Si. The formation of almost pure Cu particles explains why the Cu concentration in the matrix decreases after aging, despite the absence of Cu in Z-phase and Laves phase.

Table 3-11*. APT results of a Cu-rich particle in steel ZL1 aged for 300 h (in* ***atomic*** *percent).*

Cu	Mn	Ni	Fe	Co	Si
98.07	1.19	0.62	0.08	0.03	0.007

Figure 3-19 (a) shows APT reconstruction of a volume with a Cu-rich particle, and only Cu atoms are displayed. The size of the Cu-rich particle is larger than 30 nm, since only part of the particle was in the analysed volume. ***Figure 3-19 (b)*** shows a proxigram across the Cu/matrix interface. Ni concentration is lower compared to the surrounding matrix, while Mn concentration is higher. Interestingly, there are two concentration peaks at the interface region; in addition they do not occur at the same position relative to the interface. The Ni peak resembles a classical peak when diffusion occurs between two phases, while the peak of Mn is more likely to indicate the occurrence of interfacial segregation

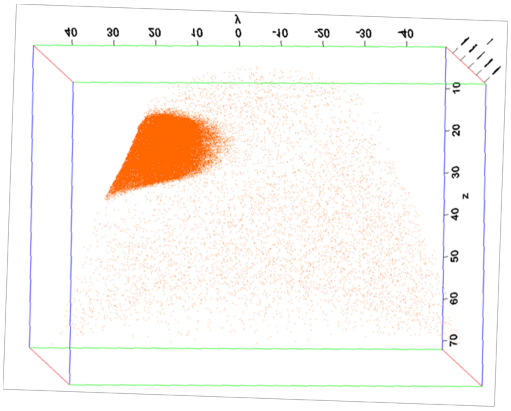

(a)

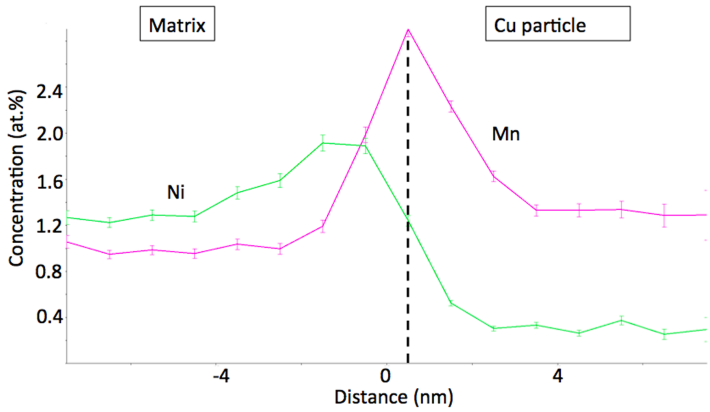

(b)

Figure 3-19. *(a) Reconstruction of an APT dataset obtained from steel ZL1 aged for 300 h. The orange dots represent Cu atoms. The size of the particle is larger than 30 nm. The box size is 100 × 100 × 72 nm^3. (b) Proxigram across the Cu/matrix interface. Note the Ni and Mn peaks in the concentration profile at the interface region.*

3.4.6.2 Secondary precipitate evolution in ZL3

Precipitate families in ZL3 are much more complicated than the Z3 and Z4 alloys. Z-phase, Ta(C,N) particles, CrN_2 particles, $M_{23}C_6$ and Cu particles are present.

Microchemistry of matrix by APT - overall precipitation reactions

The matrix chemical composition evolution of ZL3 is provided in ***Table 3-12***. A similar trend as in the Z3 and Z4 steels was also found in ZL3. N and C concentrations decrease to virtually zero even in the as-tempered condition. Obviously the full volume fraction of Z-phase, Ta(C,N), Cr_2N, and $M_{23}C_6$ has been precipitated out in the as-tempered condition. Carbon and boron are also depleted from the matrix, since their solubility in ferrite is virtually zero at the relevant temperature. During aging, the precipitates coarsen with time. Cu and Laves phase continue to nucleate and/or grow after tempering. After 1,000 hours, Cu and W concentrations remain constant. Therefore, the nucleation and growth process of Cu and Laves phase has ceased.

Table 3-12. *Chemical composition evolution of matrix for ZL3 (in* ***atomic*** *percent).*

ZL3	Fe	Cr	Co	Si	W	Cu	Mn	Ni	C	N	Ta	B
Nominal	Bal	13.1	3.34	0.62	0.76	1.73	0.22	0.18	0.28	0.20	0.11	0.03
As-tempered	82.71	12.45	3.04	0.68	0.37	0.37	0.17	0.14	0	0.003	0	0.002
1000h	82.38	12.41	3.34	0.71	0.22	0.19	0.23	0.24	0	0.001	0	0.001
5500h	81.65	12.46	3.39	0.89	0.20	0.19	0.22	0.23	0	0	0	0.001

Z-phase

Z-phase precipitates containing Ta, Cr, and N were observed in the APT analysis, see ***Figure 3-20***. They are very small, around 20 nm. The two precipitates are closely located with each other. The chemical composition of the two Z-phase particles is provided in ***Table 3-13***.

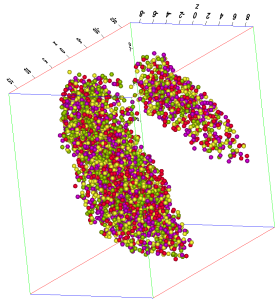

Figure 3-20*. Reconstruction of a APT dataset containing two Z-phase particles in ZL3, aged for 1,000h. Purple, yellow, red and green dots represent Ta, TaN, Cr, and N ions. Box size is 32×26×18* nm^3.

Table 3-13. *Chemical composition of Z-phase formed in ZL3 aged for 1,000 h (in* ***atomic*** *percent).*

Cr	Ta	N	Fe	C	V	B
40.8	25.8	24.5	7.0	0.6	0.8	0.2

Ta(C,N)

Two Ta(C,N) particles of ~10 and 30 nm were analysed. The chemical compositions of these two particles is provided in ***Table 3-14***. This kind of particles was also seen in ZL3 in the as-tempered condition. High C concentration in the precipitates seems to make it harder for this kind of particles to transform to Z-phase.

Table 3-14. *Chemical composition of Ta(C,N) formed in ZL3 aged for 1,000 h (in* ***atomic*** *percent).*

	Ta	C	N	Cr	Fe	V
Particle I	50.0	29.4	11.8	4.7	2.7	0.7
Particle II	43.6	35	15.5	5.0	0.5	0.5

Small Cu particles

As expected due to the poor solubility of Cu in bcc steels, Cu particles are precipitated out to the steel matrix. In the as-tempered sample, some Cu particles less than 10 nm in size were found. This is shown in ***Figure 3-21***.

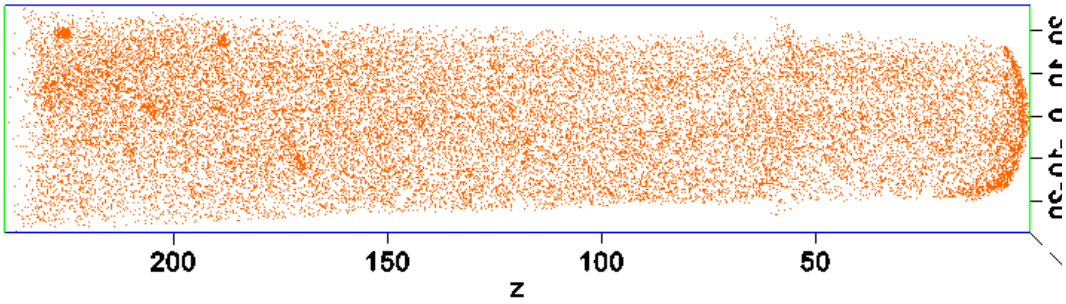

Figure 3-21. *Reconstruction of an APT dataset showing the distribution of Cu atoms. Some nano Cu particles are seen.*

SEM investigation

The secondary precipitates in ZL3 coarsen with time. After 5,500 hours aging, at least four families of precipitates can be identified: $M_{23}C_6$, Cu, Cr_xN_y, Ta(C,N) or Z-phase, and Laves phase, using SEM together with EDX. ***Figure 3-22*** shows SEM backscattered electron micrographs of the ion milled and polished thin foil of ZL3 aged for 5,500 h at different magnifications. $M_{23}C_6$ and Laves phase are located mainly along boundaries. Laves phase particles have bright contrast with a size in the range of 100-500 nm. Particles with grey contrast are mainly $M_{23}C_6$, Cu or in some rare cases CrN_2. Ta(C,N) or Z-phase precipitates also exhibit bright contrast but they are much smaller, usually less than 100 nm. Results on smaller features by TEM are presented in the following sections.

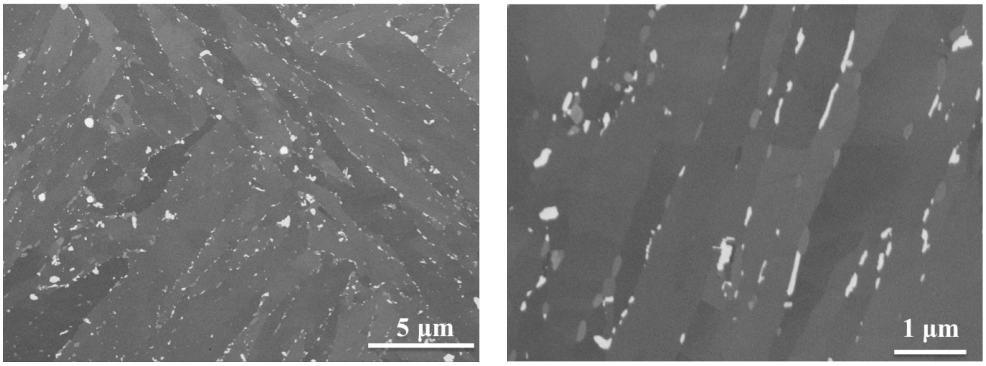

Figure 3-22. *SEM backscattered electron micrographs of ZL3 after 5500 hours ageing at 650°C.*

TEM investigation

An electropolished ZL3 as-tempered sample was studied using TEM. Note that the electrolyte preferentially etches away Cu particles and subsequently holes are left in the TEM specimens. Thus in HAADF (high angle annular dark field) micrographs (***Figure 3-23***) obtained from the electropolished specimens, the black contrast within the steel matrix is, in fact, footprints of Cu particles. Bearing in mind the fact that $M_{23}C_6$ particles and Cu particles show similar contrast in the SEM images of the bulk samples, we can consider the missing Cu particles as an advantage that makes it easy to distinguish $M_{23}C_6$ from Cu particles.

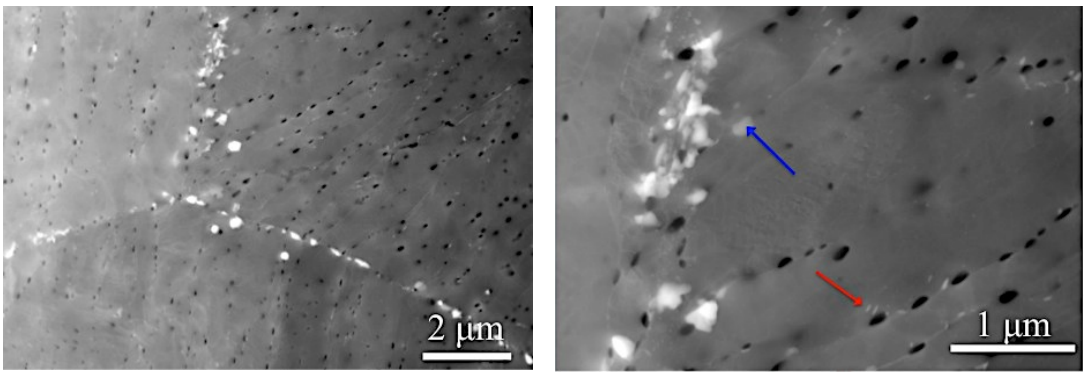

Figure 3-23. *HAADF-STEM images of ZL3 as-tempered showing Laves phase (bright contrast) and $M_{23}C_6$ (grey contrast) mostly at prior austenite grain boundaries; Ta rich particles (Z-phase and/or Ta(C,N)) marked by red arrows.*

Figure 3-24 shows STEM/HAADF micrographs of ZL3 after 1,000 h aging. It is easy to identify Laves phase (bright contrast), $M_{23}C_6$ (grey contrast) and footprints of missing Cu particles (black contrast). Note the special alignment of the footprints of Cu particles in the upper part of ***Figure 3-24 (a)***. It

indicates a special orientation relationship of Cu particles with the matrix. Small Ta-rich particles are highlighted by arrows in ***Figure 3-24 (b)***.

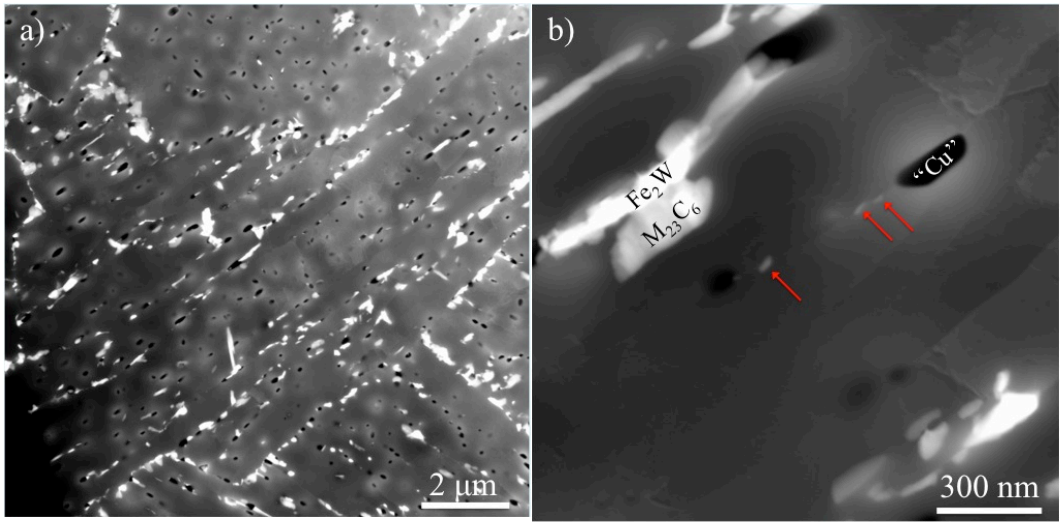

Figure 3-24. *STEM/HAADF micrographs of ZL3 1,000h-aged. (a) Laves phase with bright contrast, $M_{23}C_6$ with grey contrast, and footprint of Cu particles with dark contrast; (b) small particles rich in Ta (arrowed).*

Figure 3-25 shows STEM EDX mapping of ZL3 after 1,000 h aging. These particles are very small, less than 50 nm. All these particles are rich in both Cr and Ta. Unfortunately, the detection efficiency of the light elements such as C and N in EDX is poor. Therefore, no reliable link between Cr, Ta and C/N can be established using STEM/EDX. However, APT is capable of providing accurate chemical analysis results on both C and N as shown previously in Subsection Z-phase.

Using the ion milling and polishing method all Cu particles remain intact, and therefore, we can obtain a Cu map showing the particles, see ***Figures 3-26.*** In ***Figures 3-26***, Laves phase particles are shown by the W map. As can be seen, besides these relatively big Laves phase particles there are still particles smaller than 100 nm after 1,000 hours of ageing. Cu particles are present both along the lath boundary and inside the lath. By considering the fact that Cu particles exhibit almost the same contrast as the matrix, it is almost impossible to identify Cu particles in the HAADF micrographs. Therefore, to get good size distribution statistics on the Cu particles we suggest electropolishing as sample preparation method since it dissolves Cu particles and leave holes. Thereby, it is easy to locate them and analyse their size. Also note the arrowed Cu particle, which is surrounded by several W-rich and Cr-and, Ta-rich particles. Co-precipitation of different particles may have occurred.

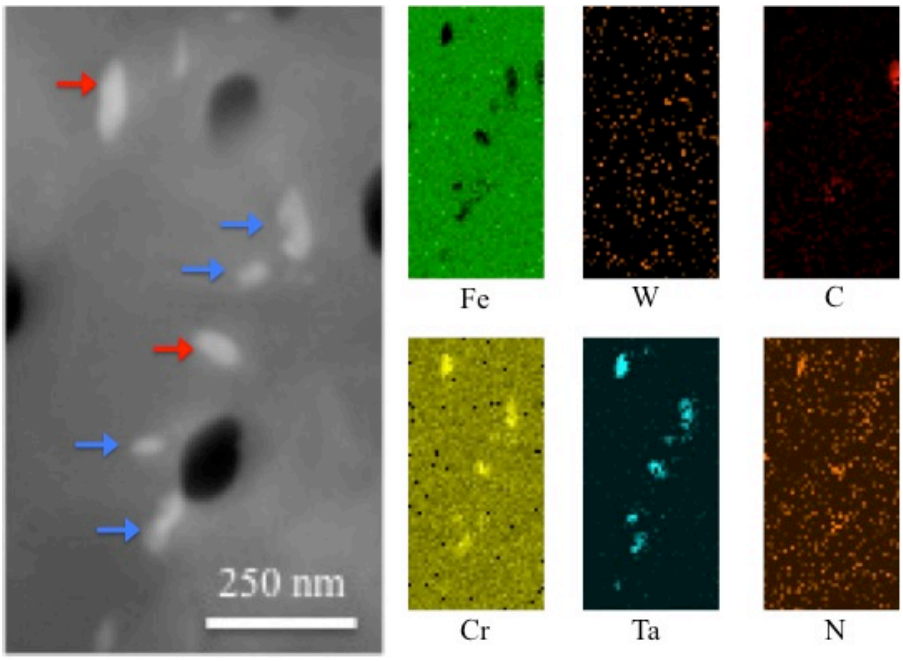

***Figure 3-25**. STEM-EDS mapping of ZL3 aged for 1000h. Red arrows point at the possible Z-phase particles and blue arrows point at Ta+Cr rich particles.*

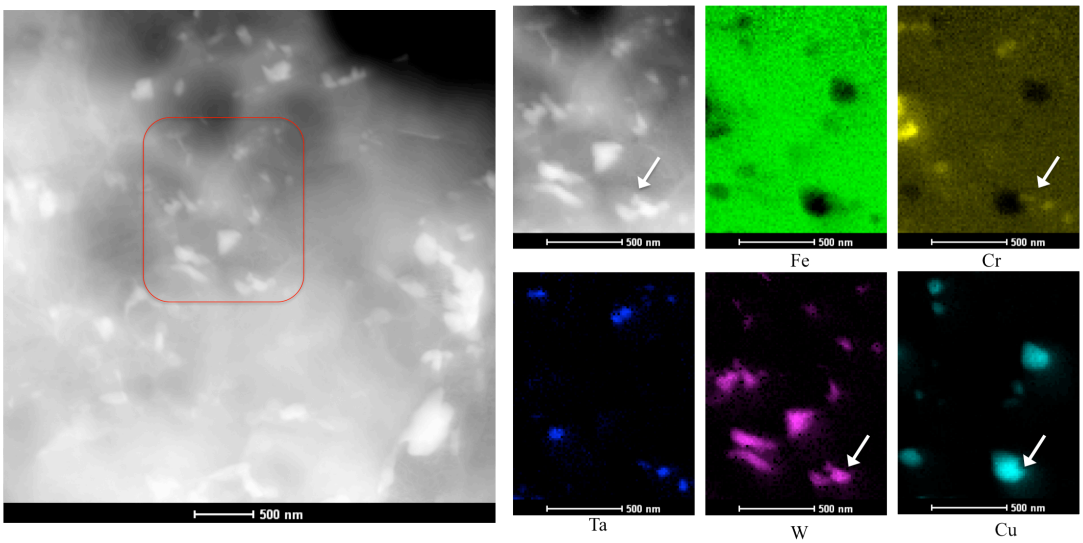

***Figure 3-26.** HAADF-STEM micrograph of ZL3 aged for 1,000 h and STEM/EDS elemental mapping of the highlighted area. There are Z-phase and Laves phase particles closely related to Cu particles.*

4 Analysis of the results

4.1 Alloy designing to avoid delta-ferrite

At the first stage of the project we started by selecting test alloys among 4 alloy chemical composition designs (Z1, Z2, Z3 and Z4) provided by DONG/DTU. Since the Cr (a ferritic stabilizer) concentration is high (actually close to the upper limit for ferritic/martensitic steels), while C (an austenitic stabilizer) concentration is lower than commonly used 9-12%Cr steels, δ-ferrite was found in test alloys Z1 and Z2. Without densely distributed strengthening precipitates, δ-ferrite is a detrimental phase for long-term creep properties at high temperatures. No noticeable δ-ferrite was found in test alloys Z3 and Z4. Therefore, they were chosen for further heat treatment optimization and mechanical testing.

For alloy designing we found that calculations based on the thermodynamic model (Thermo-Calc) alone could not give accurate prediction of the formation of δ-ferrite. We combined Thermo-Calc and a model provided by Ryu and Yu [14], and got satisfactory results. Alloy designing at the later stage was based on this combined model to predict δ-ferrite and prevent its formation in new alloys.

4.2 Primary precipitates and prior austenite grain size

PAG sizes are mainly determined by the properties of primary precipitates (TaC/NbC), i.e. the solubility of these precipitates in steels at different temperatures. In both Z4 and Z3 steels, the number of primary precipitates is small due to the low carbon content, and it decreases with increasing austenitization temperature. These precipitates can hinder the growth of PAGs during austenitization by pinning the grain boundaries. Therefore, in both alloys the average PAG size is bigger at higher austenitization temperature (***Table 3-3***). Furthermore, the PAG size is smaller in Z3 than in Z4 at 1150°C. It may be due to that at this temperature primary precipitates formed in Z3 (NbC) are less soluble than those formed in Z4 (TaC).

Z4 and ZL3 have similar chemical composition, except that ZL3 contains much more carbon (0.02at.% vs. 0.28at.%). Compared to Z4 with the same austenitization temperature, the PAG size of ZL3 is much smaller (***Table 3-4***). This is likely due to the higher C content in ZL3, and thus a larger number of primary TaC, and more pronounced grain boundary pinning by primary carbides.

4.3 General precipitation reactions

The accurate matrix chemical composition obtained using APT gives a valuable clue to the precipitation reactions. First of all, the decrease in W concentration (***Table 3-7***), combining with SEM/EDX analysis, shows evidently the formation of Laves phase. The Laves phase starts to precipitate already at the very early stage of aging. However, unlike the formation of Z-phase this process is only completed after prolonged high temperature exposure, as can be seen in all test alloys Z3, Z4 and ZL3 steel. It has been reported that Laves phase usually has a long growth period at this temperature [15]. For the nitride and carbide precipitation the full volume fraction has precipitated already after tempering.

4.4 Z-phase

Z-phase has a tetragonal crystal structure. One form of Z-phase formation occurs by continuous Cr diffusion into the metastable precursors, the pre-existing MN precipitates, as has been shown by one of the project partners DTU/DONG [16]. For CrNbN the ratio between Cr, Nb+V+Ta and N falls rather nicely to ~1:1:1. However, for CrTaN the Cr and Ta ratio is rather high: Cr:Ta ≈1.2:0.8. This ratio matches very well with what was reported by Ettmayer, who prepared and analysed tantalum Z-phase [17]. Both CrNbN and $Cr_{1+x}Ta_{1-x}N$ contain significant amount of Fe and W, which are incorporated into the precipitates probably due to their relatively high content in the matrix.

The C and B levels in the Z-phase precipitates are remarkably high, considering their extremely low concentration in the steels (0.3-0.6 at.% and 0.1-0.3 at.% in precipitates vs. 0.02 at.% in the steel). There is an interesting observation on the distribution of C and B in the Z-phase precipitates (see ***Figure 3-12***). C is distributed rather evenly in the CrNbN and $Cr_{1+x}Ta_{1-x}N$ Z-phase. This means that C might have a certain level of solubility in both types of Z-phase. In contrast, B was found enriched at the interface between the Z-phase and the matrix, which means that the solubility of B in the Z-phase is limited. The B at the interfaces is believed to be beneficial, since it may decrease the interfacial energy of the precipitates, and thus retard the coarsening of the precipitates.

Analysing small Z-phase precipitates

One issue of great concern is whether the Ta and N rich precipitates in the Z4 steel after 24 hour aging is already Z-phase or still TaN or an intermediate transient stage. Unfortunately, in this case one cannot tell directly from the APT results, despite the high spatial resolution of the instrument. This is because the precipitate atoms are smeared by the matrix atoms due to the different evaporation fields for different phases, the so-called local magnification effect [18]. We have developed a procedure for estimating chemical composition of very small Z-phase precipitates to minimize the influence from the matrix, comparing the composition of the precipitates in

the 24 h sample with the composition of those in longer time, where only Z-phase is expected. The results indicate the formation of Z-phase already after 24 hours. To confirm we must employ electron diffraction and/or the fingerprint technique in TEM/EELS for the fine electron structure of atoms, such as Cr.

4.5 Ta- vs. Nb-containing Z-phase strengthened steel

The densely distributed Z-phase precipitates can hinder the movement of boundaries and dislocations, and thus giving a better creep resistance. After tempering, both the Nb-containing Z-phase (CrNbN) strengthened steel (Z3) and the Ta-containing Z-phase (CrTaN) strengthened steel (Z4) contain densely distributed fine Z-phase precipitates (***Figure 3-13***). However, the morphology of the Z-phase precipitates in Z4 is blade-like and 10-20 nanometre in size, while in Z3 the morphology is rod-like and 10-40 nanometre in size.

The lattice parameter for CrNbN is (a=3.037 Å, c=7.391 Å) and $Cr_{1.2}Ta_{0.8}N$ is a=3.017 Å, c=7.407 Å [17], respectively. The orientation relationship between the interface of Z-phase and the steel matrix is adopted to the so-called Baker-Nutting relationship, i.e. $(001)_z \parallel (001)_{Fe}$, $[100]_z \parallel [100]_{Fe}$. The steel matrix has a body centred cubic structure with a lattice parameter of 2.866 Å. Therefore, the mismatch between CrNbN and the steel is larger than that between CrTaN and the steel. The elastic contribution to the interfacial energy is bigger for CrNbN than for CrTaN. DFT calculations performed by Fors et al. showed that the overall interfacial energy when considering both elastic and chemical contributions is larger for Fe|CrNbN than for Fe|CrTaN [19].

The experimental results of microstructure also show that the coarsening rate of CrNbN is higher than that of CrTaN after prolonged aging. Creep testing carried out by Siemens confirms that the CrTaN-strengthened Z4 steel performs better in terms of creep. That Ta tends to form finer precipitates compared to Nb was also reported by Wang and her co-workers, who aimed to use Ta and Nb to form MX precipitates in their experimental 9-12% Cr steels. They found that Ta-containing MX precipitates are finer compared to the Nb-containing MX precipitates in another steel [20].

4.6 Effects of Cu addition on Laves phase at prior austenite boundaries

Tensile and impact testing were performed on Z3 and Z4 samples. Both steels exhibited very good tensile strength ($R_{p0.2}$ around 800 MPa) and ductility (elongation at fracture >15%) (**Table 3-5**). However, they showed very poor impact toughness. We believed that preferential segregation of W and/or consequently precipitation of Laves phase particles along prior austenite grain boundaries and lath boundaries were responsible for the poor impact strength

for Z3 and Z4 (***Figure 3-16***). To modify kinetics and distribution of Laves phase formation we added Cu.

There have been extensive studies on Cu additions to high-strength steels, where due to its low solubility in ferrite Cu tends to form precipitates, which can act as one of the major hardening agents. In these steels Cu precipitates are often observed to undergo several stages of phase transformation, from metastable body-cantered cubic (bcc) structure to intermediate 9R structure and gradually into face-cantered cubic equilibrium structure of pure Cu [21]. In 9-12%Cr steels, Cu addition can effectively avoid the formation of delta ferrite, which is detrimental to the mechanical properties of the steels. In addition, Cu precipitates may provide nucleation sites for Laves phase formation [22].

In fact the improved toughness in ZL series steels by Cu addition is, most likely, related to suppression of preferential precipitation of embrittling Laves phase along prior austenite grain boundaries of the steel in the as tempered condition [23]. Laves phase tends to nucleate heterogeneously along boundaries. Other types of precipitate like $M_{23}C_6$ can greatly influence the nucleation process of Laves, and subsequently the number density and size of Laves phase particles. It takes a long time for the precipitation of Laves phase to reach its equilibrium volume fraction [24]. O. Prat et al. reported approximately 1.5 years at 650°C in a 9%Cr steel [25].

Since there was no Cu partitioning into the Laves phase found, it is expected that Cu precipitates may have similar effect on Laves phase as $M_{23}C_6$. Cu tends to precipitate out very quickly, and form nano-sized precipitates at grain/lath boundaries and dislocations. On one hand Cu nano-particles may occupy the possible nucleation sites, which otherwise can be occupied by Laves phase. On the other hand, since Cu precipitates much more rapidly than Laves phase, Cu particles can provide a large number of new potential nucleation sites for Laves phase. A large number of Laves phase particles can be formed on Cu particles, and thus leading to a much denser distribution of Laves phase particles. However, Z-phase, the major precipitate phase in steel Z4, does not have such effect on Laves phase.

With regard to the morphology of the Laves phase, it is speculated that there is crystallographic orientation between Cu particles, most probably in coherent bcc structure, and the α-ferrite matrix, and subsequently between Cu particles and Laves particles that nucleated upon them. These Laves phase particles may then grow along a certain direction, which is more energetically beneficial. Ku et al. also reported rod-shaped morphology [22] in a Cu-containing 9%Cr steel. Furthermore, they showed a Cu particle connected to a Laves phase particle. Besides Cu addition, heat treatment is also essential for the morphology since probably only Cu particles with certain crystallographic structure can introduce Laves phase with a certain orientation relationship. Further investigation on heat treatment conditions and in detailed TEM study are planned.

Another possibility is that the exchange of 0.12 at.% (of a total of 0.89 at.%) of W for Mo might change the lattice parameter of Laves phase somewhat, decreasing the elastic part of the interfacial energy and thus facilitating

nucleation, assuming then that nucleation occurs in a coherent fashion relative to the matrix or Cu particles. Also the chemical part of the interfacial energy could possibly be affected by the change in Laves phase chemistry, but it seems unlikely that this could be a large effect.

4.7 Effect of C addition

One effect of "normal" amount of C addition is to form a large number of primary precipitate carbides, and thus pinning the prior austenite grain boundaries and yield a smaller grain size. This effect is clearly shown by the much smaller prior austenite grain size compared with Z4 with the same austenitization temperature.

The second effect of C addition is the formation of different families of secondary carbides and carbonitrides, such as $M_{23}C_6$ and Ta(C,N). $M_{23}C_6$ has long been considered as one of the most efficient beneficial precipitates for creep resistance, with its coarsening constant between MX and Laves phase. Small $M_{23}C_6$ at prior austenite grain boundaries are considered essential to ensure a good creep resistance, the so-called grain boundary strengthening [26]. When B is added the coarsening constant of $M_{23}C_6$ becomes much smaller. In collaboration with Professor Göran Wahnström and his co-workers, who performed ab-initio calculations, we revealed that the B can retard the coarsening of $M_{23}C_6$. Atomistic modelling showed that boron diffusion in ferrite is dominated by an interstitial mechanism at 600°C. However, the generation of vacancies when carbide precipitates dissolve may promote a distribution with substitutional boron atoms. The absence of a fast mechanism for the transition from substitutional to interstitial occupancy will make the slow substitutional boron diffusion in the matrix rate controlling for the coarsening process.

C addition also influences the kinetics of Z-phase formation. With a low C concentration, such as in test steels Z3 and Z4, Z-phase formed during a short period of time of about 24 hours. With a high C concentration, such as in ZL3, small Z-phase particles co-exist with other carbonitrides. These carbonitrides are relatively stable, and were observed in samples aged for 1,000 hours. Obviously, these particles cannot be transformed to Z-phase readily. The effect of these precipitates on the creep properties of the steels is still under investigation.

5 Conclusions

We have proved that the concept of using finely distributed Z-phase to strengthen 12% chromium steels for higher service temperatures up to 650°C is feasible.

Compared to Nb, Ta is a better candidate to form fine Z-phase precipitates in 12% chromium steels. The Ta test steel was comparable with the benchmark P92 (that has only 9% Cr), and the Nb test steel was comparable to P91.

Continuous Laves phase precipitates formed along prior austenite boundaries are detrimental to the impact toughness of the new steels. By adding Cu, the distribution of Laves phase is largely modified, and thus leading to desirable impact toughness. An addition of alloying element Cu has a significant influence on the behaviour of Laves phase. It reduces Laves phase formation along prior austenite grain boundaries, thus improving the toughness of the steel. It also changes the morphology of Laves phase precipitates from rather coarse equiaxied to densely distributed rod-shaped. The later morphology is stable at least up to 1000 hours. The formation of this type of morphology is believed to be due to the nucleation of Laves phase upon nano-sized Cu precipitates, since Cu does not partition to Laves phase.

Addition of C into the alloy system gives a less expensive steel (a lower Co content) but leads to a much more complicated microstructure with the formation of many types of nano-sized carbides and nitrides in addition to Z-phase. Their effect on creep strength is not known yet, but creep tests have started.

6 Goal fulfilment

- Select test steels;

We have selected testing alloy Z3, Z4 and ZL3 from seven candidates alloys for further mechanical testing and microstructure analysis.

- Creep testing on promising test steels;

We have performed long-term creep testing on the selected testing alloys Z3, Z4 and ZL3. Some of the experiment is still on going (which is very good, since it means the steels we developed are strong at high temperatures.)

- Understand mechanisms of accelerated Z-phase formation by Ta addition;

The difference is most likely caused by a smaller total interfacial energy of Ta-based Z-phase.

- Understand effects of small addition of B on the Z-phase strengthened steels;

The distribution map of B was obtained. Their effect lies in their enrichment at Z-phase interface and thus decreasing the interface energy.

- Understand microstructure of Z-phase strengthened steels with different heat treatments.

The effect of C and microstructure under different heat treatment conditions were investigated.

7 Suggestions for future research work

Through this project, together with our partners within the closely related projects financed by the Swedish Energy Agency (Fundamental Energy Research in Cooperation with VR), Research foundation of VGB in Germany, and FP7, we have shown that very fine Z-phase precipitates can densely distributed in the new steels and efficiently strengthen the steels. At elevated temperatures good creep properties that are comparable with today's best commercial creep resistant 9-12% Cr steels – P92, have been achieved, with good corrosion properties ensured by their high Cr content.

In order to implement this new generation of steels in future power plants, the following three aspects needs to be addressed.

1. Fine tune alloy designing

The next step is to fine tune the alloy composition and make it stronger at 650°C. This must be done by combining modelling and experimental tools.

2. Establish modelling

To predict the long-term behaviour of the steels, reliable modelling must be established. For the moment, thermodynamic database for the important component in the steel, Ta, is largely lacking. Experiments play an essential role in verifying modelling to ensure the quality of modelling.

8 Literature references

[1] International Energy Agency, http://www.iea.org, 2009.
[2] International Energy Agency, International Energy Agency, France, 2012.
[3] K. Maruyama, K. Sawada, J.-i. Koike, ISIJ International, 41 (2001) 641-653.
[4] M. Taneike, F. Abe, K. Sawada, Nature, 424 (2003) 294-296.
[5] T. Fujita, ISIJ International, 32 (1992) 175-181.
[6] A.J. Sedriks, Chapter 10: Corrosion by hot gases and molten compounds, Corrosion of stainless steels, A Wiley-Interscience publication John Wiley & Sons, Inc., 1996.
[7] T. Uehara, A. Toji, S. Komatsubara, T. Fujita, in: J. Lecomte-Beckers, M. Carton, F. Schubert, P.J. Ennis (Eds.) Materials for advanced power engineering, Forschungszentrum Jülich GmbH, Liege, Belgium, 2002, pp. 1311-1320.
[8] A. Strang, V. Vodarek, Materials Science and Technology, 12 (1996) 552-556.
[9] M. Svoboda, J. Bursik, I. Podstranska, A. Krouppa, V. Sklenicka, K.H. Mayer, in: J. Lecomte-Beckers, M. Carton, F. Schubert, P.J. Ennis (Eds.) Materials for advanced power engineering, Forschungszentrum Jülich GmbH, Liege, Belgium, 2002, pp. 1521-1530.
[10] H. Danielsen, J. Hald, VGB Power Tech, (2009) 1-6.
[11] W.O. Binder, Symposium on sigma-phase, Cleveland, OH, 1950, pp. 146.
[12] M. Hättestrand, M. Schwind, H.-O. Andren, Materials Science and Engineering A, A250 (1998) 27-36.
[13] F. Abe, International Journal of Materials Research, (2008) 387-394.
[14] S.H. Ryu, J. Yu, Metallurgical and Materials Transactions a-Physical Metallurgy and Materials Science, 29 (1998) 1573-1578.
[15] L. Korcakova, Department of manufacturing engineering and management, Technical University of Denmark, 2002.
[16] H.K. Danielsen, J. Hald, M.A.J. Somers, Scripta Materialia, 66 (2012) 261-264.
[17] P. Ettmayer, Monatshefte für Chemie / Chemical Monthly, 102 (1971) 858-863.
[18] M.K. Miller, Atom probe tomography - analysis at the atomic level, Kluwer Academic/Plenum Publishers, 2000, pp. 151.
[19] D.H.R. Fors, G. Wahnstrom, Journal of Applied Physics, 109 (2011) 113709.
[20] Y. Wang, K.-H. Mayer, A. Scholz, C. Berger, H. Chilukuru, K. Durst, W. Blum, Materials Science and Engineering A, 510-511 (2009) 180-184.
[21] D. Isheim, M.S. Gagliano, M.E. Fine, D.N. Seidman, Acta Materialia, 54 (2006) 841-849.
[22] B.S. Ku, J. Yu, Scripta Materialia, 45 (2001) 205-211.
[23] Morris J.W.Jr., Z. Guo, C.R. Krenn, Y.-H. Kim, ISIJ International, 41 (2001) 599-611.

[24] M. Hättestrand, H.-O. Andrén, Materials Science and Engineering A - Structural Materials Properties Microstructure and Processing, 318 (2001) 94-101.
[25] O. Prat, J. Garcia, D. Rojas, G. Sauthoff, G. Inden, Intermetallics, 32 (2013) 362-372.
[26] F. Abe, Strengthening mechanisms in steel for creep and creep rupture, in: A. F, K. T-U, R. Viswanathan (Eds.) Creep-resistant steels, Woodhead Publishing Limited, 2008, pp. 279-301.
[27] http://imagej.nih.gov/ij/index.html, 2011.

9 Publications

A comprehensive understanding on this new generation of martensitic steels has been gain through all the efforts by the project partners. Part of the results has been disseminated through publication in high impact scientific journals, or international conferences. A few high quality scientific papers presenting the original results are under preparation for the moment.

1. Atomic resolution imaging of precipitate transformation from cubic TaN to tetragonal CrTaN
Hilmar K. Danielsen, John Hald, Marcel A.J. Somers,
Scripta Materialia, Volume 66, Issue 5, March 2012, Pages 261-264

2. Microstructure evolution of a Z-phase strengthened 9-12% Cr steel
Hans-Olof Andrén, Fang Liu
The 8th International Charles Parsons Turbine Conference, Portsmouth, UK, September 5th - 8th, 2011.

3. Understanding of 9-12% Cr steels on a nano- and subnano-scale – the secret of TAF
Hans-Olof Andrén, Fang Liu
Invited talk
2nd International Conference on Super-High Strength Steels, Peschiera del Garda Italy, October 17th - 20th, 2011.

4. Effects of laser pulsing on analysis of steels by atom probe tomography
Fang Liu, Hans-Olof Andrén
Ultramicroscopy, Vol. 111, 633-641, 2011.

5. Effect of Boron on Carbide Coarsening at 873 K (600 °C) in 9 to 12 pct Chromium Steels
Fang Liu, Dan H.R. Fors, Ardeshir Golpayegani, Hans-Olof Andrén and Göran Wahnström
Metallurgical and Materials Transactions A, Vol. 43, 4053-4062, 2012

6. Effect of Cu addition on the toughness of new Z-phase strengthened 12% Cr steels
Fang Liu, Hans-Olof Andrén
EPRI 7th International Conference on Advances in Materials Technology for Fossil Power Plants, October 22 -25, 2013.

7. The effect of C and Cu addition on the microstructure of Z-phase strengthened 9-12% Cr steels
Masoud Rashidi, Fang Liu, Hans-Olof Andrén
10th Liège Conference on Materials for Advanced Power Engineering, September 14th – 17th, 2014, Liège, Belgium, accepted.

Appendices

Experimental methods

1. Materials preparation

The test steels were produced in 80 kg ingots by Vacuum Induction Melting (VIM) process. The ingots were hot rolled into 20 mm thick plates, and subsequently followed by different quality heat treatment conditions: austenitization, quenching, and tempering.

2. Mechanical testing

All mechanical testing were conducted according to corresponding European testing standard listed in Table A1.

Table A1. *Standards used for mechanical testing.*

Type of testing	Standard
Hardness	EN ISO 6507-1:2005 (30 kg load)
Impact	EN ISO 148-1:2010
Tensile testing at room temperature	EN ISO 6892-1:2009
Tensile testing at elevated temperatures	EN ISO 6892-2:2011
Interrupted and uninterrupted creep rupture testing	EN ISO 204:2009

Interrupted creep rupture tests were carried out at 625°C with nominal stresses of 150, 125, 100 and 75 MPa, using specimens of approx. 5 mm in diameter and 30 mm in gauge length. Uninterrupted creep rupture tests were carried out at 650°C with nominal stresses of 120, 100 and 80 MPa, using specimens of approximately 7 mm in diameter and 50 mm in gauge length.

3. Sample preparation for SEM

The SEM samples were prepared by mechanical polishing on a polishing machine: ground and polished until 1 micrometre diamond spray, and finishing with 0.25 micrometre colloidal SiO_2 suspension.

4. Sample preparation for TEM

TEM specimens were prepared by the standard electropolishing method. The steels were first cut to ~0.25 mm thin slices using a low speed saw, and then mechanical polished down to ~0.05 mm. Then the polished thin slice was punched to 3 mm discs, followed by electropolishing in an electrolyte of 10% perchloric acid in methanol at -35°C.

5. Sample preparation for APT

The steels were cut into small rods (~ 8 × 0.25 × 0.25 mm^3) by a low speed saw. The rods underwent a two-step electropolishing procedure in order to obtain APT samples with a final radius of less than 50 nm. First a thin neck was produced in 10% perchloric acid in methanol. Then fine polishing was made in a bath of 2% perchloric acid in 2-butoxyethanol until the lower part of the rod dropped off. All the APT samples were examined in a Leo Ultra 55 Field Emission Gun Scanning Electron Microscope (FEG-SEM) before being investigated in the atom probe.

6. SEM

The prepared SEM samples were examined in a Leo Ultra 55 Field Emission Gun Scanning Electron Microscope (FEG-SEM). Chemical analysis was done by the Oxford Inca Energy Dispersive X-ray Spectrometry (EDX) system fitted to the SEM. The operation voltage was at 20 kV.

7. TEM

A Philips CM200 FEG TEM and a TECNAI (200 kV) equipped with an EDX were used to characterize microstructure of the Z-phase strengthened steels.

8. Atom probe tomography

In order to analyse the chemical composition of the matrix as well as the small precipitates of the steels an Imago LEAP 3000X HR local electrode atom probe instrument was used. The sample temperature during analysis was in the range of 55-65K. For the Nb-containing steel, the pulsed voltage mode was used with a pulse fraction of 20%. To avoid premature specimen failure for Ta-containing steel pulsed laser mode was used, with a laser energy of 0.3 nJ. The acquired data were further analysed by using the IVAS^{TM} software developed by Imago.

9. Proxigram

In order to obtain accurate chemical information across certain interface, we used the so-called proxigram (proximity histogram), an embedded function in the APT reconstruction program. Here we explain how this function works. To get the chemical composition across an interface, we can take a volume, e.g. a cylinder, which includes the interface, which is often defined by the continuous surface with the same concentration for certain element, the so-called iso-concentration surface. Then we calculate the concentration data along the height. It is very important that the direction of the height of cylinder is perpendicular to the interface plane, in order to avoid smearing of the interface concentration. However, since the interfaces are usually irregular, it is often impossible to define just one volume, which covers the entire interface and simultaneously has the height perpendicular to the entire interface. What the proxigram algorithm does is to create a very small cylinder, make it move over the entire interface, while changing its position to

ensure that it is perpendicular to the interfaces, calculate the concentration and finally integrate it over for the entire interface. In this way, a composition profile over the interfaces with much less smearing is obtained.

10. Image process and analysis

The image process software Image J [27] was used for analysing SEM secondary electron images. A threshold was set and applied for each SEM images in order to convert them to binary images for analysis. Information about precipitate number, size and area fraction was stored in a text file, which was then handled using Excel.

ELFORSK

SVENSKA ELFÖRETAGENS FORSKNINGS- OCH UTVECKLINGS - ELFORSK - AB

Elforsk AB, 101 53 Stockholm. Besöksadress: Olof Palmes Gata 31
Telefon: 08-677 25 30, Telefax: 08-677 25 35
www.elforsk.se